Biologically induced initiation of Neoproterozoic snowball-Earth events

Eli Tziperman[a,1], Itay Halevy[b], David T. Johnston[a], Andrew H. Knoll[a], and Daniel P. Schrag[a]

[a]Department of Earth and Planetary Sciences, Harvard University, 20 Oxford Street, Cambridge, MA 02138; and [b]Division of Geological and Planetary Sciences, California Institute of Technology, MC 100-23, 1200 East California Boulevard, Pasadena, CA 91125

Edited by Timothy W. Lyons, University of California, Riverside, CA, and accepted by the Editorial Board July 12, 2011 (received for review November 11, 2010)

The glaciations of the Neoproterozoic Era (1,000 to 542 MyBP) were preceded by dramatically light C isotopic excursions preserved in preglacial deposits. Standard explanations of these excursions involve remineralization of isotopically light organic matter and imply strong enhancement of atmospheric CO_2 greenhouse gas concentration, apparently inconsistent with the glaciations that followed. We examine a scenario in which the isotopic signal, as well as the global glaciation, result from enhanced export of organic matter from the upper ocean into anoxic subsurface waters and sediments. The organic matter undergoes anoxic remineralization at depth via either sulfate- or iron-reducing bacteria. In both cases, this can lead to changes in carbonate alkalinity and dissolved inorganic pool that efficiently lower the atmospheric CO_2 concentration, possibly plunging Earth into an ice age. This scenario predicts enhanced deposition of calcium carbonate, the formation of siderite, and an increase in ocean pH, all of which are consistent with recent observations. Late Neoproterozoic diversification of marine eukaryotes may have facilitated the episodic enhancement of export of organic matter from the upper ocean, by causing a greater proportion of organic matter to be partitioned as particulate aggregates that can sink more efficiently, via increased cell size, biomineralization or increased C:N of eukaryotic phytoplankton. The scenario explains isotopic excursions that are correlated or uncorrelated with snowball initiation, and suggests that increasing atmospheric oxygen concentrations and a progressive oxygenation of the subsurface ocean helped to prevent snowball glaciation on the Phanerozoic Earth.

carbon isotopes | CO_2

Between 750 and 580 million years (My) ago, the Earth experienced multiple ice ages, two of which deposited glaciogenic sediments in equatorial seas (1–3). These "snowball" glacial records have no equivalent in younger successions, and, indeed, there is little evidence for continental ice sheets of any kind in the preceding 1,500 My. A runaway ice albedo can lead to global glaciation once sea ice crosses a critical latitude of about 30 to 40°. However, the initial trigger that led to a critical extent of sea ice cover is far from obvious, although many potential drivers have been proposed (4). Solar luminosity was 7% lower than at present, yet this by itself cannot constitute the needed trigger because luminosity was even lower during earlier periods when no glaciation is recorded. The stratigraphic distribution of glaciogenic rocks thus presents two questions of timing. First, why are unusually severe ice ages limited to the observed interval of later Neoproterozoic time? And second, what initiated discrete and repeated episodes of global glaciation within this interval?.

Tectonic arguments have been proposed to explain the first of these questions via the triggering of carbon cycle feedbacks. Later Neoproterozoic rifting, supercontinent breakup and low-latitude continents provided mechanisms for enhanced organic carbon burial and, hence, drawdown of atmospheric CO_2 (3–6). Neoproterozoic concentration of highly reflecting continental area near the equator reduced the absorption of solar radiation (2), while also eliminating the negative feedback between CO_2 abundance and the rate of chemical weathering, which would otherwise occur via the glaciation of higher-latitude continents (4). Finally, low-latitude continents might strengthen chemical weathering by exposing continental areas to high precipitation rates and high temperature (3). However, these tectonic arguments do not explain what prevented the Earth from plunging into another snowball as soon as one was over, given that continental drift is slow relative to the time scale of the carbon cycle feedbacks being triggered.

The two most extensive Neoproterozoic glaciations were preceded by a distinct excursion of carbon isotopic values in carbonate rocks (the pre-Sturtian Islay anomaly and the pre-Marinoan Trezona anomaly); in each case, $\delta^{13}C$ declined more than 10 permil, from strongly positive values broadly characteristic of early Neoproterozoic carbonates (7, 8) to negative values rarely observed in rocks of any age. The duration of the preglaciation isotopic excursions is not well constrained, but the Trezona anomaly in Namibia, for example, is estimated from tectonic subsidence rates to have come and gone on the order of 0.5–1 My (9). It has been argued that the excursions were caused by a decrease in the organic carbon burial fraction (3), a decrease in productivity relative to carbonate deposition due to ocean cooling (3), a rapid turnover of poorly ventilated deep oceans (10), or the oxidation of a large organic carbon reservoir (11). Although all of these mechanisms could, in principle, cause $\delta^{13}C$ values to decline, most could enhance atmospheric CO_2, making them unlikely triggers for glaciation.

In some Neoproterozoic successions, the isotopic excursions are recorded in carbonate rocks but not in associated organic carbon (11–13). However, recent evidence (14) suggests that $\delta^{13}C$ of the organic and inorganic pools covaried through at least some of these excursions. Although it is possible that the dramatic presnowball $\delta^{13}C$ excursions (8) are not related to the glaciation or may even be diagenetic (15–17), the proximity of the two in several geological records suggests that we must consider the possibility that they are related. If related to the snowball events, the $\delta^{13}C$ excursions may indicate that the marine biosphere underwent major changes prior to snowball events. In order to explain both a snowball initiation and the preglaciation isotopic signal with a single mechanism, Schrag et al (4) considered a slow but sustained release of methane from isotopically light, deep ocean methane clathrates.

Here, we consider an alternative possibility, that the snowball events and isotopic excursions were both triggered by biological changes involving marine microorganisms via anaerobic remineralization of organic matter. Motivated by recent findings (11, 18, 19), we also present variants of the scenario in which glaciation could be triggered by the marine biosphere without producing an

Author contributions: E.T. designed research; E.T., I.H., D.T.J., A.H.K., and D.P.S. performed research; and E.T., I.H., D.T.J., A.H.K., and D.P.S. wrote the paper.

The authors declare no conflict of interest.

This article is a PNAS Direct Submission. T.W.L. is a guest editor invited by the Editorial Board.

[1]To whom correspondence should be addressed. E-mail: eli@eps.harvard.edu.

This article contains supporting information online at www.pnas.org/lookup/suppl/doi:10.1073/pnas.1016361108/-/DCSupplemental.

isotopic excursion and vice versa. The mechanism, although necessarily speculative, may explain why snowball events occurred in the Neoproterozoic but not thereafter, addresses the time scale between events, seems consistent with snowball-related geochemical observations, and makes several testable predictions.

An Overview of the Snowball Initiation Scenario

First, we consider attempts to explain preglacial isotopic excursions by a net aerobic remineralization of isotopically light organic matter. Fig. 1 shows such a scenario (using the model described in *Materials and Methods* and the *SI Appendix*). The scenario assumes a temporary drop in oxygenic primary production while aerobic remineralization proceeds unchanged (Fig. 1*A*). The pool of dissolved organic carbon (DOC) consequently shrinks while the dissolved inorganic carbon (DIC) pool grows (Fig. 1*B*), and the isotopic composition of both becomes significantly lighter (Fig. 1*B*). However, as a result of the increased DIC pool, atmospheric pCO_2 rises dramatically (Fig. 1*C*), preventing glaciation and, therefore, seemingly inconsistent with the observed record.

There are many indications that the oxygen minimum zone of Neoproterozoic oceans tended toward anoxia (20, 21). With this in mind, we consider a steady state of ocean biogeochemistry, with oxygenic upper ocean primary production by cyanobacteria and algae balanced largely by aerobic remineralization within the surface ocean mixed layer. A (small) net export production flux would maintain subsurface water-column anoxia by consuming dissolved oxygen mixed into the subsurface ocean from oxygenated surface water. Most of the organic matter would be contained within the upper oxygenated ocean in both dissolved form and suspended particulate form (e.g., cyanobacteria cells) that tends to remain in the upper ocean because of its relative buoyancy; both forms are referred to together below as DOC. Further consider the possibility that at some point an increase in this export rate sends an enhanced flux of organic matter into anoxic subsurface waters and sediments, where it could be remineralized to dissolved inorganic carbon via anaerobic respiration by either sulfate reducing bacteria or iron-reducing bacteria, or buried.

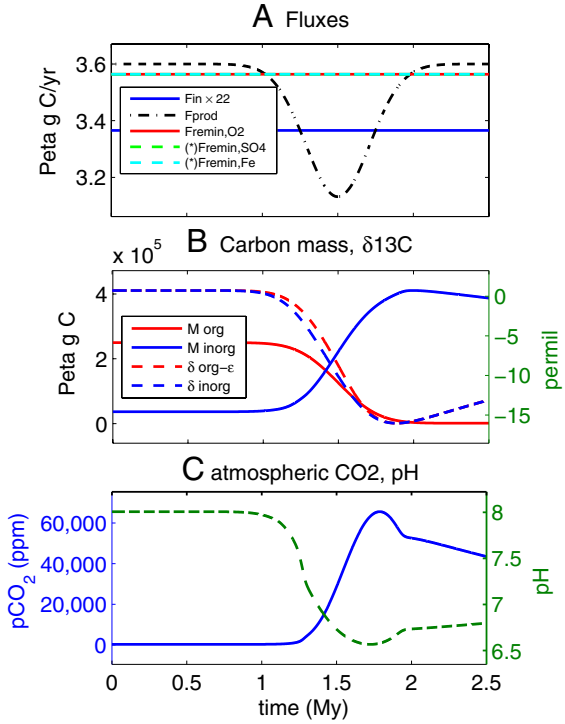

Fig. 1. Time-dependent results of scenario #1, a net aerobic remineralization of organic matter leading to a negative $\delta^{13}C$ isotopic excursion. Time advances from left to right. (*A*) Prescribed carbon fluxes; the only flux prescribed to change in this scenario is the decreasing oxygenic production F_{prod} forcing the isotopic signal. (*) Anaerobic remineralization fluxes are plotted shifted and are identically zero in this scenario. (*B*) Dissolved organic and inorganic carbon masses (solid lines) and $\delta^{13}C$ isotopic compositions (dashed). (*C*) Atmospheric pCO_2 (ppm) showing a large increase, due to the increase in dissolved inorganic carbon concentration, and a decrease in ocean pH.

Enhanced export production causes partially oxygenated subsurface ocean layers to be stripped of oxygen by the enhanced aerobic remineralization of sinking organic matter. This extends the depth range through which anoxic conditions dominate and may, therefore, reduce both oxygenic production and aerobic remineralization. As we will see shortly, this combination can lead to a reduction of atmospheric pCO_2 as well as a carbon isotopic signal consistent with the observed presnowball excursions. To appreciate this, examine now how these processes affect the marine carbonate system. Production and remineralization in the upper ocean may be represented by

$$2CO_2 + 2H_2O \rightleftharpoons 2CH_2O + 2O_2. \quad [1]$$

Next, the anoxic remineralization of organic matter via sulfate (SO_4^{2-}) reduction leads to the formation of sulfide (H_2S, or in its dissociated form, HS^-). Sulfide can either diffuse toward the oxygenated upper ocean and be oxidized back into sulfate, or react with Fe^{2+} to form pyrite. These three processes may be represented by

$$\begin{aligned} &2CH_2O + SO_4^{2-} \rightarrow HS^- + H_2O + CO_2 + HCO_3^-, \\ &HS^- + 2O_2 \rightarrow SO_4^{2-} + H^+, \\ &Fe^{2+} + 2HS^- \rightarrow FeS_2 + H_2. \end{aligned} \quad [2]$$

Sulfate reduction can take place in anoxic subsurface water, although the sediments are a more likely site because of the higher organic matter concentrations and longer exposure time there (22). Next, examine the effect of sulfate reduction on the carbonate system and therefore on atmospheric pCO_2 (schematically shown on the right side of Fig. 2). If the induced reduction in aerobic remineralization is exactly balanced by anoxic remineralization via sulfate reduction, there is no net change in remineralization, and the scenario is effectively described by reaction **2a** minus reaction **1**,

$$SO_4^{2-} + CO_2 + H_2O \rightarrow HS^- + HCO_3^- + 2O_2.$$

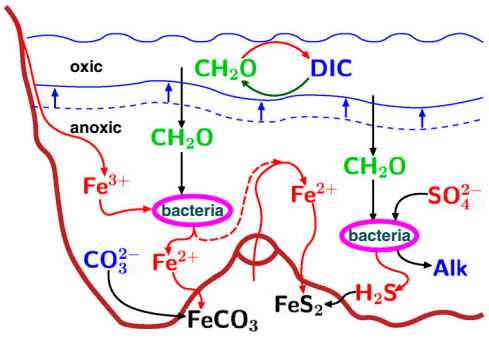

Fig. 2. Schematic of the biologically induced snowball initiation scenarios. The right side represents the sulfate reduction plus pyrite formation pathway, which increases alkalinity and therefore reduces pCO_2; the left side represents the iron reduction path, which leads to the deposition of siderite and reduction in the size of the DIC pool, and therefore, again, to the reduction of pCO_2. Note the shoaling of the (dashed blue) interface between the anoxic and oxic ocean depth ranges, in response to the enhanced export production, potentially leading to a reduction of both oxygenic production and aerobic remineralization. These scenarios are demonstrated using a single box model described in the text.

Thus, the net reaction involves no change to the organic (CH_2O) or inorganic (CO_2, HCO_3^-) carbon pools, but leads to a significant addition of carbonate alkalinity via the addition of HCO_3^-. (Alkalinity may be defined as net charge due to ions of weak acids involved in the carbonate system; a useful approximation for the purpose of this section is $Alk = [HCO_3^-] + 2[CO_3^{2-}] + [OH^-] - [H^+]$; see *Materials and Methods* for details). An interesting consequence of the above scenario is that the added alkalinity leads to a reduction of the atmospheric pCO_2 (23), which may provide a biological mechanism for snowball initiation.

In order for a negative isotopic excursion to develop as well, a net remineralization of isotopically light organic matter is required, due to either increased remineralization rates or a drop in oxygenic production. This is a fine balance, as the net remineralization adds to the DIC pool and therefore tends to increase the pCO_2. For a reduction in atmospheric pCO_2 to accompany an isotopic signal, the increase in alkalinity due to anaerobic remineralization must exceed the increase in the size of the DIC pool. This is demonstrated using specific time-dependent model scenarios in the next section.

If the sulfide (H_2S) formed by sulfate reduction within the sediments diffuses upward into the oxygenated ocean water, and is oxidized via reaction **2b**, the carbonate alkalinity gained by sulfate reduction is lost and there is no reduction in atmospheric CO_2. However, if the sulfide reacts with Fe^{2+} to form pyrite via reaction **2c** within the sediments or within anoxic subsurface water masses, the alkalinity is retained. Below, we assume that 50% of the sulfide generated by bacterial sulfate reduction is removed by pyrite formation and that the rest is oxidized. Note that pyrite formation is a complex multistage process that is not completely understood. Arguments have been raised for (24–26) and against (27, 28) the reaction **2c** used above, which is the net reaction of a complex multistage process. The *SI Appendix*, section SI-3, cites literature suggesting that this net reaction is a viable path in the presence of biological catalysts. Alternative pyrite formation scenarios to [**2c**] may lead to the removal of alkalinity added during sulfate reduction and eliminate the pCO_2 reduction (*SI Appendix*, section SI-3).

Next, consider a similar scenario involving anoxic remineralization of exported organic matter into DIC by iron-respiring bacteria reducing Fe^{3+} to Fe^{2+}. This reaction may again be followed by either mixing of Fe^{2+} toward the upper ocean and its oxidation back into Fe^{3+}, or by siderite ($FeCO_3$) formation and burial. These three reactions are represented by

$$2CH_2O + 8Fe(OH)_3 \rightarrow 8Fe^{2+} + 2HCO_3^- + 14OH^- + 6H_2O,$$
$$8Fe^{2+} + 2O_2 + 20H_2O \rightarrow 8Fe(OH)_3 + 16H^+,$$
$$8Fe^{2+} + 8CO_3^{2-} \rightarrow 8FeCO_3. \quad [3]$$

Dissimilatory iron reduction of organic matter [**3a**] leads to a large injection of sixteen carbonate alkalinity units (via the $14OH^-$ and $2HCO_3^-$ terms) per two units of remineralized organic matter—while increasing the DIC by only two (via $2HCO_3^-$). This would lead to a reduction of pCO_2, except that once the Fe^{2+} is oxidized to Fe^{3+} via [**3b**] or reacts with the carbonate ion to form siderite via [**3c**], the entire alkalinity addition is lost. In the latter case, some DIC is deposited as siderite, which does lead to a reduction of pCO_2.

Next, we consider specific model calculations based on the above scenarios. Although clearly not quantitative because of the many uncertainties regarding Neoproterozoic conditions, the results below are nonetheless useful in allowing us to visualize the above scenarios and examine their consequences.

Results of a Time-Dependent Scenario

The model is described in *Materials and Methods* and the *SI Appendix*. The results of the main scenario, involving both sulfate and iron reduction, are summarized in Fig. 3. Fig. 3*A* shows the prescribed fluxes that drive the isotopic signal and atmospheric CO_2 drawdown. Export production is specified to increase over a time period of about 0.5 My, and then recover. In response, for the reasons explained above, both oxygenic primary production and aerobic remineralization are prescribed to decrease (dashed black and red curves). In parallel, exported organic matter is remineralized by sulfate reduction and iron reduction (dashed cyan and green).

The changes in productivity and remineralization fluxes correspond to a net remineralization, which leads to a decrease of the organic matter pool, which is converted to DIC (Fig. 3*C*). We find that we need to postulate a large initial organic matter pool (13), about 400 times larger than that of present day, to allow for a net remineralization event large enough to explain the observed isotopic signal. The net remineralization leads to a large isotopic excursion of DIC, 15‰ (Fig. 3*C*), and the isotopic compositions of the DOC covary with DIC as the latter is incorporated into newly produced DOC. This covariation is consistent with recent measurements of Neoproterozoic samples (14). Ref. 13 also assumed the DOC pool to be large, to prevent it from covarying with the DIC. This was motivated by earlier measurements indicating no such covariation (12). The carbonate system (Fig. 3*B*) responds to the changes in DIC, alkalinity fluxes, and enhanced DIC burial (below), leading to a significant CO_2 drawdown (Fig. 3*I*).

A major issue for the scenario considered here is the availability of sufficient sulfate and iron (see also ref. 29). Fig. 3*D* indicates that some 6 millimol per liter (mM) sulfate are needed, or, equivalently, that the maximum required sulfate flux into the ocean at the peak of the event be about four times the present-day flux. The Neoproterozoic ocean was most likely sulfate poor (30), with probably no more than about 10% of the present-day concentration of 28 mM. Recent arguments suggest higher sulfate concentrations can be maintained during ferruginous conditions (21), and are supported by sulfate evaporite deposition (31). A level of approximately 3 mM before the beginning of the event, supplemented by riverine continental flux about twice that the of present day, could provide sufficient sulfate. Enhanced continental weathering due to continental collision and building of a supercontinent could provide the additional flux. Providing the implied Fe^{2+} flux for pyrite formation (solid blue curve in Fig. 3*E*, peaking at approximately 10×10^{12} mol/y) seems more of a challenge. Estimates of Fe^{2+} released today by midoceanic ridges vary between 2×10^{11} mol/y (32) and 9×10^8 mol/y (33). However, given the lower sulfate concentration in the Neoproterozoic, the hydrothermal Fe^{2+} concentration is expected to have been much higher (34). In addition, a somewhat higher-than-present Neoproterozoic heat flux could have lead to a higher hydrothermal water flow, consistent with trace element measurements (35) that suggest a high ratio of hydrothermal to riverine input to the ocean in the late Proterozoic. The higher heat flux also implies higher temperatures in hydrothermal systems, which could lead to a hundredfold increase in the Fe^{2+} flux (36), bringing the required Fe^{2+} flux for pyrite formation within reach. The mechanisms suggested here for an increased Fe^{2+} supply to the ocean, although speculative, are consistent with iron speciation chemistry, which suggests that beginning about 800 My ago, anoxic subsurface waters were commonly ferruginous (20, 21). Finally, the required Fe^{3+} flux for iron reduction (solid red in Fig. 3*E*) peaks at (only) about 3 times present-day flux into the ocean (dashed red) and may result again from tectonically enhanced weathering associated with continental collision and building of a supercontinent (37). In addition, Fe^{3+} can accumulate in sediments before the beginning of the event and be used there by iron-reducing bacteria (38) during the event, so that the required amount of Fe^{3+} again does not seem to contradict existing information about iron availability.

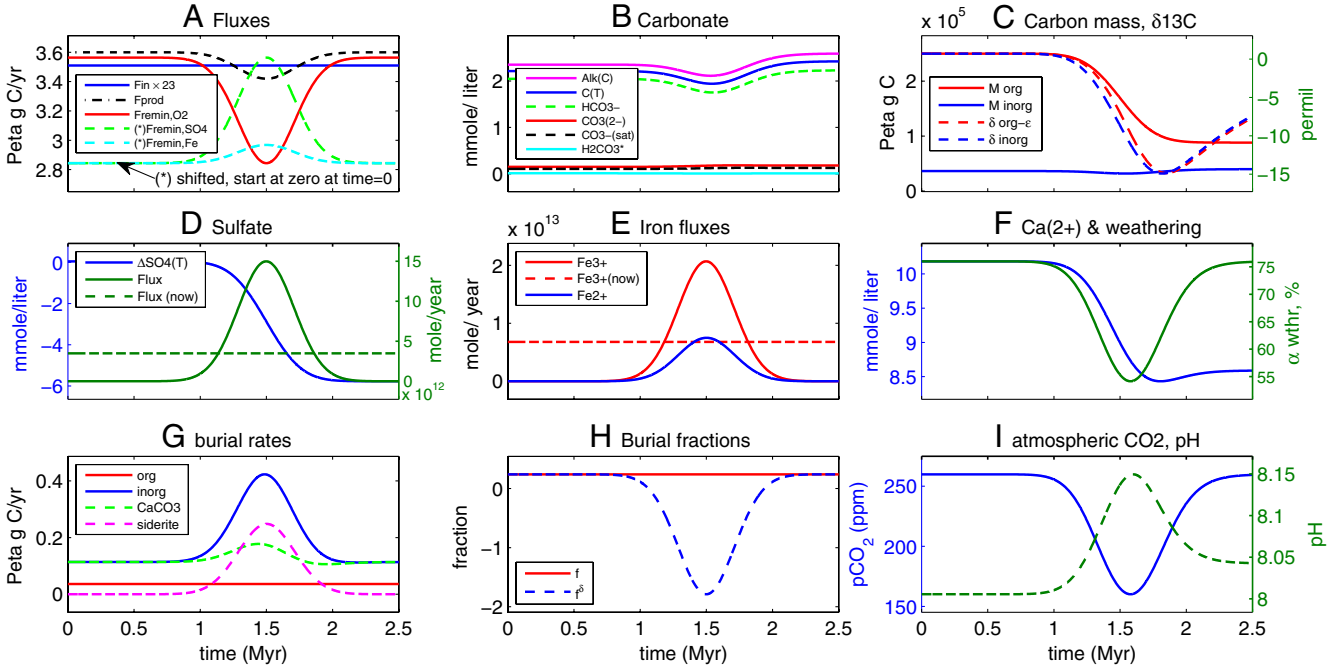

Fig. 3. Time-dependent model scenario (#2) of snowball initiation. (*A*) Prescribed carbon fluxes, due to oxygenic production (F_{prod}), aerobic remineralization (F_{remin,O_2}), input from volcanoes and carbonate weathering (F_{in}, multiplied by 23), sulfate remineralization ($F_{remin,SO4}$) and iron reduction ($F_{remin,Fe}$). (*) The last two fluxes, representing anaerobic remineralization, are plotted shifted and their initial value before the anomaly is zero. (*B*) Carbonate speciation. (*C*) Organic and inorganic carbon masses (solid lines) and $\delta^{13}C$ isotopic composition (dash). (*D*) Decrease in sulfate concentration [$\Delta SO_4(T)$, blue], or, alternatively, the required sulfate flux into the ocean (green, solid) for the sulfate reduction scenario. The present-day riverine flux is shown by the green, dashed line. (*E*) Implied iron fluxes of Fe^{3+} for iron reduction part of the scenario (red, with present-day flux into the ocean shown in red dashed line), and the implied flux of Fe^{2+} for the sulfate reduction and pyrite formation (blue). (*F*) Organic and inorganic burial rates. (*G*) Ca^{2+} and the weathering fraction α_{wthr} (*SI Appendix*). (*H*) Organic burial fraction f and non-steady-state fraction f^{δ} defined in the text. (*I*) Atmospheric CO_2 and ocean pH.

The low-latitude Neoproterozoic land mass distribution (39) could make the tropical oceans especially rich in iron and phosphate carried from the continents. Much of the biological production, anoxic remineralization, and exchange of CO_2 with the atmosphere may have therefore been concentrated in low-latitude seas. In this case, the relevant ocean volume participating in setting the atmospheric CO_2 could have been much smaller. The fluxes of iron and sulfate required to affect the carbonate system of this smaller ocean volume could be significantly reduced, making the scenario more realizable.

In aerobic scenarios of DOC remineralization, ocean pH decreases because of an increase in the size of the marine DIC pool, leading to enhanced dissolution of marine carbonates. The current scenario (Fig. 3*G*) predicts instead an increased rate of carbonate deposition during the isotopic excursion, due to increased alkalinity and pH. Intensified DIC burial, which disposes of the newly produced DIC and allows the drawdown of atmospheric CO_2, is divided between deposition of calcium carbonate (with a corresponding decrease in Ca^{2+} concentration, Fig. 3*F*) and siderite.

The large isotopic signal found here is possible because of a deviation from steady-state dynamics (see a related discussion in ref. 13). If the DOC pool is not as large as assumed in ref. 13, it is likely in an isotopic quasi-equilibrium ($d\delta_{org}/dt \approx 0$) because of its short residence time. The isotopic compositions are then governed by (*Materials and Methods*) $\delta_{org} = \delta_{inorg} + \varepsilon$ and

$$M_{inorg}\frac{d\delta_{inorg}}{dt} = F_{in}(\delta_{in} - \delta_{inorg}) - (F_{prod} - F_{remin})\varepsilon, \qquad [4]$$

where $\varepsilon = -28‰$ is the fractionation between organic and inorganic matter, M_{inorg} is the DIC pool, F_{prod} is the organic matter production rate, F_{remin} is the total remineralization rate, F_{in} is the carbon flux from volcanoes and carbonate weathering, and δ_{in} is its isotopic composition. At the minimum point of an inorganic isotopic excursion, where $\frac{d}{dt}\delta_{inorg} = 0$, we therefore have $\delta_{inorg} = \delta_{in} - f^{\delta}\varepsilon$, with $f^{\delta} = (F_{prod} - F_{remin})/F_{in}$. In a steady state, $F_{prod} - F_{remin}$ is the organic burial rate and f^{δ} is then the organic burial fraction, f. But in a non-steady-state of the DIC pool, remineralization could significantly outpace primary production, making f^{δ} negative and large (Fig. 3*H*), leading to a large negative isotopic excursion (Fig. 3*C*) not possible in a steady state, when $f^{\delta} = f > 0$.

Fig. 3*I* shows the ocean pH increasing during the event, and the pCO_2 decreasing. Recent model estimates for the threshold CO_2 leading to a snowball vary from below present-day values to four times present-day values (40). We demonstrate that a pCO_2 reduction in conjunction with an appropriate isotopic signal is indeed possible under the specified scenario, and a much larger pCO_2 reduction is easily obtained by retuning the model. Given the enormous increase in pCO_2 in the standard aerobic remineralization scenario for explaining the isotopic signal (Fig. 1), it is remarkable that a self-consistent scenario invoking anaerobic remineralization can produce an isotopic excursion of as much as 15‰ as well as a significant decrease in pCO_2 (Fig. 3 *C* and *I*). This provides a counterview to organic matter oxidation acting as a negative feedback preventing a full glaciation (41).

Carbon fluxes due to production and remineralization are prescribed rather than calculated from first principles here, because of uncertainties regarding Neoproterozoic biogeochemistry. We therefore consider in the *SI Appendix*, section SI-4, a fairly thorough set of sensitivity tests of our results to changes in prescribed fluxes, demonstrating the robustness of the model results to prescribed parameters.

Discussion and Comparison to Available Observations

This paper is motivated by a 200-My period of time, characterized by several major glacial events and isotope anomalies of distinct character. Given the simplicity of the model used here, it is best

not to attempt to model specific glaciations and isotopic anomalies found in the geologic record. Still, the scenario considered here may explain observed large negative presnowball $\delta^{13}C$ excursions, while accounting for a reduction in atmospheric pCO_2 that could lead to global glaciations. It also makes additional predictions that can be tested against the geologic record. Both the sulfate and iron reduction paths lead to an increased ocean pH (Fig. 3*I*). This modest pH increase represents an ocean-wide average, and could have been larger in some specific environments. Evidence of increased pH may be found in unusual centimeter-scale talc nodules formed during early diagenesis of carbonate sediments, observed to date only in mid-Neoproterozoic marine successions and requiring pore water pH > 8.6 (42). The increased pH also leads to a prediction of enhanced calcium carbonate deposition (Fig. 3*G*), consistent with the observation of widespread stromatolite formation in immediately preglacial successions (43). The model uncertainty does not allow us to determine whether the DIC deposition via siderite or carbonate precipitation may have dominated during the preglacial Neoproterozoic (Fig. 3*G*), yet both rates may be expected to be significant, in particular on anoxic continental shelves and slopes where organic carbon accumulates. Indeed shales deposited in anoxic shelf environments suggest that all deposited carbonates are siderite (a few percent of total deposits) (21), although it is difficult to estimate global budgets. We do not have a record of still deeper environments, and although preserved shallow-water environments show abundance of carbonate, they show little to no siderite, perhaps because they were oxygenated. Overall, geochemical observations of later Neoproterozoic sedimentary rocks seem consistent with the requirements and predictions of the scenario considered here.

Some recent observations show the large negative isotopic $\delta^{13}C$ excursions returning to positive values prior to the regional onset of glacial deposits (11, 18, 19). Moreover, the late Ediacaran Shuram anomaly is the largest in the geological record and appears to postdate the Neoproterozoic glaciations. This raises the interesting possibility that the $\delta^{13}C$ excursions and snowball events are not mechanistically linked. By changing the balance between iron reduction and sulfate reduction on one hand, and oxygenic production and aerobic remineralization on the other, the above scenario may be modified to result in a CO_2 reduction without a $\delta^{13}C$ signal, as well as an isotopic signal without CO_2 change (scenarios #5 and #6 in the *SI Appendix*, section SI-4; Figs. SI-5 and SI-6).

The oxygenic fixation of organic matter, followed by anaerobic remineralization, amounts to an oxygen source. The sulfide and iron oxidation act as oxygen sinks. The net oxygen source predicted here thus needs to be regulated by appropriate sinks so that the deep ocean remains anoxic for the above scenario to be valid. The implied O_2 source is significant, of the same order as present-day pyrite weathering and volcanogenic (via SO_2 gas) sink of O_2 (*SI Appendix*, section SI-5), seemingly allowing for the possibility of such regulation, except that weathering flux before the advent of land plants may have been as much as one order of magnitude weaker. All we can currently do is point out this significant difficulty with the scenario examined here.

Conclusions

We examined whether an enhanced export production scenario followed by anoxic remineralization of the sinking organic matter may lead to isotopic excursions as observed before the two largest Neoproterozoic glaciations. Specifically, sulfate reduction followed by pyrite formation increases alkalinity and therefore enhances calcium carbonate precipitation. Alkalinity gained during iron reduction is lost during the siderite formation that follows, but siderite formation itself leads to DIC burial. In both cases, and unlike the explanation of the isotopic signal via aerobic remineralization, the net effect can lead to a drawdown rather than a large increase of atmospheric pCO_2, possibly explaining both the isotopic signal and snowball initiation. Previously proposed mechanisms for ice age initiation (see the Introduction) may all supplement the scenario discussed here and are not inconsistent with it.

The factors that could lead to enhanced export production, and thus initiate the above scenario, remain conjectural. It is interesting to note, however, that although eukaryotes originated early in the Proterozoic Eon, if not earlier, both fossils (44) and molecular biomarkers (45) show evidence of dramatic increase in the abundance, diversity, and environmental distribution of marine eukaryotes beginning about 800 My ago. Biogeochemical consequences potentially include higher sinking rates on continental shelves, associated with larger mean cell size and propensity to form particulate aggregates (46); higher sinking rates associated with mineralized tests and scales (45, 47); and increased biomass associated with high (relative to cyanobacteria) C:N in eukaryotic phytoplankton (48). Thus, mid-Neoproterozoic increase in the importance of marine eukaryotes could have provided marine ecosystems with an unprecedented capacity for episodic increases in export flux. Therefore, given the increased vulnerability of the Earth system to glaciation introduced by tectonic factors, episodically enhanced increase in the export of organic matter into anoxic subsurface water masses and sediments could have pushed climate beyond the threshold for glaciations, and done so repeatedly. If later Ediacaran oceans were more broadly oxygenated (49), the biological mechanism introduced here for glacial initiation would no longer apply. The anaerobic remineralization mechanism considered here may be relevant to other carbon isotopic excursions in Earth history that did not necessarily involve the large pCO_2 increases expected from large-scale aerobic remineralization events. Although hypothetical and speculative, many aspects of the mechanisms considered here are testable, and it should be interesting to examine the geologic record in view of these ideas.

Materials and Methods

The model considers the ocean as a single volume, yet treats separately anoxic and oxic remineralization processes. The organic carbon mass (particulate and dissolved) is affected by primary production, total remineralization and burial, $dM_{org}/dt = F_{prod} - F_{remin} - F_{b,org}$, whereas the inorganic carbon mass is affected in addition by volcanic input, $dM_{inorg}/dt = F_{in} + F_{remin} - F_{prod} - F_{b,inorg}$. The organic and inorganic isotopic compositions are governed by $M_{org}d\delta_{org}/dt = F_{prod}(\delta_{inorg} + \varepsilon - \delta_{org})$ and $M_{inorg}d\delta_{inorg}/dt = F_{in}(\delta_{in} - \delta_{inorg}) - (F_{prod} - F_{remin})\varepsilon - F_{remin}(\delta_{inorg} + \varepsilon - \delta_{org})$, where ε represents the fractionation during biological production. The model includes an expanded carbonate system with the carbonate species, $CO_2(g) \rightleftharpoons H_2CO_3^*$, $H_2O \rightleftharpoons H^+ + OH^-$, $H_2CO_3^* \rightleftharpoons H^+ + HCO_3^-$, $HCO_3^- \rightleftharpoons H^+ + CO_3^{-2}$; boron, $B(OH)_3 + H_2O \rightleftharpoons H^+ + B(OH)_4^-$; sulfate and sulfide, $HSO_4^- \rightleftharpoons H^+ + SO_4^{2-}$, $H_2S(aq) \rightleftharpoons HS^- + H^+$. These are solved for at every time step to round-off accuracy using Jacobian-assisted optimization (*SI Appendix*, section SI-2.10), and given the values of total dissolved CO_2, boron, sulfide, and sulfate and a generalized alkalinity (charge balance), all defined as follows, $C_T = [H_2CO_3^*] + [HCO_3^-] + [CO_3^{-2}]$, $B_T = [B(OH)_4^-] + [B(OH)_3]$, $S_T = [HSO_4^-] + [SO_4^{2-}]$, $(H_2S)_T = [H_2S(aq)] + [HS^-]$, $Alk_G = [HCO_3^-] + 2[CO_3^{-2}] + [B(OH)_4^-] + [HSO_4^-] + 2[SO_4^{2-}] + [HS^-] + [OH^-] - [H^+]$. The total CO_2 is given by the inorganic carbon mass M_{inorg} per liter; total boron is specified at 400 μmol/L; total sulfide and sulfate concentrations are affected by sulfate remineralization flux, by the mixing of sulfide toward upper oxic ocean and its eventual oxidation back to sulfate, and by pyrite formation, $d(H_2S)_T/dt = +\frac{1}{2}F_{remin,SO_4} - F_{H_2S,mixing} - F_{pyrite}$, $dS_T/dt = -0.5F_{remin,SO_4} + F_{H_2S,mixing}$. Generalized alkalinity sources and sinks include the input weathering flux of calcium carbonate, inorganic burial, pyrite formation, iron remineralization, and mixing followed by oxidation of iron and siderite formation, $dAlk_G/dt = 2 \times \alpha_{wthr}F_{in} - 2 \times F_{b,inorg} - F_{pyrite} + 8F_{remin,Fe} - 2F_{Fe,mixing} - 2F_{siderite}$. The effect of the weathering feedback on alkalinity input, α_{wthr}, follows ref. 50. The calcium ion concentration is affected by input weathering flux and sedimentation/dissolution of $CaCO_2$, $dCa^{2+}/dt = F_{in,Ca^{2+}} - F_{b,inorg}$. Iron(III) is consumed by iron remineralization and produced by mixing and oxidation of iron(II), $dFe^{3+}/dt = -4F_{remin,Fe} + F_{Fe,mixing}$. Iron(II) budget is additionally affected by siderite formation, $dFe^{2+}/dt = 4F_{remin,Fe} - F_{siderite} -$

$F_{Fe,mixing}$. The prescribed fluxes have a Gaussian structure in time (*SI Appendix*, section SI-2.2). The response to step-forcing is examined in the *SI Appendix*, where the model is also fully described, and the response amplitude is found to be remarkably robust, although its temporal structure does depend on that of the forcing. The model code is written in Matlab and is available with the *SI Appendix* or at www.seas.harvard.edu/climate/eli/Downloads.

ACKNOWLEDGMENTS. We thank Timothy Lyons, Chris Reinhard, and two anonymous reviewers for most constructive and helpful comments. We are grateful for helpful discussions and comments from Arren Bar-Even, Don Canfield, Hezi Gildor, Peter Huybers, Francis Macdonald, Ron Milo, and Aldo Shemesh. This work was supported by National Science Foundation Grant ATM-0902844 (to E.T.) and National Aeronautics and Space Administration Grant NNX07AV51 (to A.H.K. and D.T.J.). E.T. thanks the Weizmann Institute for its hospitality during parts of this work.

1. Harland WB (1964) *Problems in Palaeoclimatology*, ed AEM Nairn (John Wiley & Sons, London), pp 119–149 pp 180–184.
2. Kirschvink J (1992) *The Proterozoic Biosphere: A Multidisciplinary Study*, eds J Schopf and C Klein (Cambridge Univ Press, Cambridge, U.K.), pp 51–52.
3. Hoffman PF, Kaufman AJ, Halverson GP, Schrag DP (1998) A Neoproterozoic snowball Earth. *Science* 281:1342–1346.
4. Schrag DP, Berner RA, Hoffman PF, Halverson GP (2002) On the initiation of a snowball Earth. *Geochem Geophys Geosyst* 3:1036.
5. Knoll AH (1992) *The Origin and Early Evolution of Metazoans*, ed JL Signor P (Plenum, New York), pp 53–84.
6. Godderis Y, et al. (2007) Coupled modeling of global carbon cycle and climate in the Neoproterozoic: Links between Rodinia breakup and major glaciations. *C R Geosci*, pp:212–222.
7. Knoll AH, Hayes JM, Kaufman AJ, Swett K, Lambert IB (1986) Secular variation in carbon isotope ratios from upper Proterozoic successions of Svalbard and East Greenland. *Nature* 321:832–838.
8. Halverson GP, Wade BP, Hurtgen MT, Barovich KM (2010) Neoproterozoic chemostratigraphy. *Precambrian Res* 182:337–350.
9. Halverson GP, Hoffman PF, Schrag DP, Kaufman AJ (2002) A major perturbation of the carbon cycle before the Ghaub glaciation (Neoproterozoic) in Namibia: Prelude to snowball Earth? *Geochem Geophys Geosyst* 3:1035.
10. Kaufman AJ, Knoll AH, Narbonne GM (1997) Isotopes, ice ages, and terminal Proterozoic Earth history. *Proc Natl Acad Sci USA* 94:6600–6605.
11. Swanson-Hysell NL, et al. (2010) Cryogenian glaciation and the onset of carbon-isotope decoupling. *Science* 328:608–611.
12. Hayes JM, Strauss H, Kaufman AJ (1999) The abundance of C-13 in marine organic matter and isotopic fractionation in the global biogeochemical cycle of carbon during the past 800 Ma. *Chem Geol* 161:103–125.
13. Rothman DH, Hayes JM, Summons RE (2003) Dynamics of the Neoproterozoic carbon cycle. *Proc Natl Acad Sci USA* 100:8124–8129.
14. Johnston DT, et al. (2010) New insight into the character of the Neoproterozoic carbon cycle. *Geological Society of America Abstracts with Programs* 42:395.
15. Derry LA (2010) A burial diagenesis origin for the Ediacaran Shuram-Wonoka carbon isotope anomaly. *Earth Planet Sci Lett* 294:152–162.
16. Knauth LP, Kennedy MJ (2009) The late Precambrian greening of the Earth. *Nature* 460:728–732.
17. Swart PK, Kennedy M (2010) A comparison of the Trezona carbon anomaly with the Plio-Pleistocene. *Geological Society of America Abstracts with Programs* 42:396.
18. Macdonald FA, Jones DS, Schrag DP (2009) Stratigraphic and tectonic implications of a newly discovered glacial diamictite-cap carbonate couplet in southwestern Mongolia. *Geology* 37:123–126.
19. Macdonald FA, et al. (2010) Calibrating the Cryogenian. *Science* 327:1241–1243.
20. Canfield D, et al. (2008) Ferruginous conditions dominated later Neoproterozoic deep water chemistry. *Science* 321:949–952.
21. Johnston DT, et al. (2010) An emerging picture of Neoproterozoic ocean chemistry: Insights from the Chuar Group, Grand Canyon, USA. *Earth Planet Sci Lett* 290:64–73.
22. Neretin LN, Bottcher ME, Grinenko VA (2003) Sulfur isotope geochemistry of the Black Sea water column. *Chem Geol* 200:59–69.
23. Zeebe R, Wolf-Gladrow D (2001) *CO_2 in Seawater: Equilibrium, Kinetics, Isotopes*, (Elsevier, Amsterdam), Elsevier Oceanography Series, Vol. 65.
24. Rickard D, Luther GW, III (2007) Chemistry of iron sulfides. *Chem Rev* 107:514–562.
25. Drobner E, Huber H, Wachtershauser G, Rose D, Stetter KO (1990) Pyrite formation linked with hydrogen evolution under anaerobic conditions. *Nature* 346:742–744.
26. Donald R, Southam G (1999) Low temperature anaerobic bacterial diagenesis of ferrous monosulfide to pyrite. *Geochim Cosmochim Acta* 63:2019–2023.
27. Berner RA (1970) Sedimentary pyrite formation. *Am J Sci* 268:1–23.
28. Benning LG, Wilkin RT, Barnes HL (2000) Reaction pathways in the Fe-S system below 100 degrees C. *Chem Geol* 167:25–51.
29. Bristow TF, Kennedy MJ (2008) Carbon isotope excursions and the oxidant budget of the Ediacaran atmosphere and ocean. *Geology* 36:863–866.
30. Hurtgen MT, Arthur MA, Suits NS, Kaufman AJ (2002) The sulfur isotopic composition of Neoproterozoic seawater sulfate: Implications for a snowball Earth? *Earth Planet Sci Lett* 203:413–429.
31. Rainbird RH, Jefferson CW, Young GM (1996) The early Neoproterozoic sedimentary succession B of northwestern Laurentia: Correlations and paleogeographic significance. *Geol Soc Am Bull* 108:454–470.
32. Elderfield H, Schultz A (1996) Mid-ocean ridge hydrothermal fluxes and the chemical composition of the ocean. *Annu Rev Earth Planet Sci* 24:191–224.
33. Tagliabue A, et al. (2010) Hydrothermal contribution to the oceanic dissolved iron inventory. *Nat Geosci* 3:252–256.
34. Kump LR, Seyfried WE (2005) Hydrothermal Fe fluxes during the Precambrian: Effect of low oceanic sulfate concentrations and low hydrostatic pressure on the composition of black smokers. *Earth Planet Sci Lett* 235:654–662.
35. Derry L, Jacobsen S (1988) The Nd and Sr isotopic evolution of Proterozoic seawater. *Geophys Res Lett* 15:397–400.
36. Seyfried WE, Janecky DR (1985) Heavy-metal and sulfur transport during subcritical and supercritical hydrothermal alteration of basalt—influence of fluid pressure and basalt composition and crystallinity. *Geochim Cosmochim Acta* 49:2545–2560.
37. Tosca NJ, et al. (2010) Clay mineralogy, organic carbon burial, and redox evolution in Proterozoic oceans. *Geochim Cosmochim Acta* 74:1579–1592.
38. Dong H, Jaisi DP, Kim J, Zhang G (2009) Microbe-clay mineral interactions. *Am Mineral* 94:1505–1519.
39. Hoffman PF, Li ZX (2009) A palaeogeographic context for Neoproterozoic glaciation. *Palaeogeogr Palaeoclimatol Palaeoecol* 277:158–172.
40. Voigt A, Abbot DS, Pierrehumbert RT, Marotzke J (2010) Initiation of a Marinoan snowball Earth in a state-of-the-art atmosphere-ocean general circulation model. *Clim Past Discuss* 6:1853–1894.
41. Peltier WR, Liu Y, Crowley JW (2007) Snowball earth prevention by dissolved organic carbon remineralization. *Nature* 450 813-U1.
42. Tosca NJ, Macdonald FA, Strauss JV, Johnston DT, Knoll AH (2011) Sedimentary talc in Neoproterozoic carbonate successions. *Earth Planet Sci Lett* 306:11–22.
43. Hoffman PF (2011) Strange bedfellows: Glacial diamictite and cap carbonate from the Marinoan (635) glaciation in Namibia. *Sedimentology* 58:57–119.
44. Knoll AH, Javaux E, Hewitt D, Cohen P (2006) Eukaryotic organisms in Proterozoic oceans. *Philos Trans R Soc Lond B Biol Sci* 361B:1023–1038.
45. Cohen PA, Schopf JW, Butterfield NJ, Kudryavtsev AB, Macdonald FA (2011) Phosphate biomineralization in mid-Neoproterozoic protists. *Geology* 39:539–542.
46. Burd AB, Jackson GA (2009) Particle aggregation. *Ann Rev Mar Sci* 1:65–90.
47. Porter SM, Knoll AH (2000) Testate amoebae in the Neoproterozoic era: Evidence from vase-shaped microfossils in the Chuar Group, Grand Canyon. *Paleobiology* 26:360–385.
48. Nagy RM, Porter SM, Dehler CM, Shen Y (2009) Biotic turnover driven by eutrophication before the Sturtian low-latitude glaciation. *Nat Geosci* 2:414–417.
49. Canfield DE, Poulton SW, Narbonne GM (2007) Late-Neoproterozoic deep-ocean oxygenation and the rise of animal life. *Science* 315:92–95.
50. Berner R (1994) GEOCARB-II—A revised model of atmospheric CO^2 over Phanerozoic time. *Am J Sci* 294:56–91.

Supplementary Information for: Biologically induced snowball initiation

Eli Tziperman [*] **Itay Halevy** [†] **David T. Johnston** [*] **Andrew H. Knoll** [*] **and Daniel P. Schrag** [*]

[*]Dept of Earth and Planetary Sciences, Harvard University, 20 Oxford St, Cambridge, MA, 02138, and [†]Div. of Geological & Planetary Sciences, Caltech, MC 100-23 1200 E. California Blvd., Pasadena, CA, 91125

Prepared using PNAS LaTeX package, submitted to Proceedings of the National Academy of Sciences of the United States of America

SI-1. Overview

The supplementary information is divided into the model formulation (SI-2), a discussion of pyrite formation (SI-3), some additional scenarios supplementing those discussed in the main text and extensive sensitivity tests (SI-4), a calculation of the implications on the oxygen cycle (SI-5) and some back of the envelope calculations verifying model results (SI-6).

SI-2. Model formulation

We start the model description with a discussion of the carbon mass balance and isotopic mass balance equations (section SI-2.1), and then describe the specific scenario modeled here, specifying the changes to the export production, oxygenic production rate, aerobic remineralization rate and anaerobic remineralization rates (SI-2.2). The equations (dissociation reactions) for the expanded carbonate system are then described, including the carbonate system, boron, sulfate and sulfide (SI-2.3). Because the remineralization of organic matter leads to pH changes, it is essential to include the buffering effect via the dissolution of bottom sediments (SI-2.4). This, in turn, requires that we include the chemical weathering feedback as well for consistency (SI-2.5). The Ca^{2+} ion concentration may change significantly due to dissolution and deposition, and is therefore also added as a prognostic variable (SI-2.6). Next, sulfate reduction is discussed, including the pyrite formation sink for the sulfide formed by sulfate reduction (SI-2.7), and followed by iron reduction and siderite formation (SI-2.8). Several of the processes listed above contribute to carbonate alkalinity changes, which in turn plays a critical role in setting the atmospheric CO_2 concentration, and the corresponding charge budget is presented (SI-2.9). The solution method of the expanded carbonate system is described in (SI-2.10), including both an exact numerical solution and an approximate solution which provides some intuition into the effects of the alkalinity changes due to sulfate reduction.

The model parameters that are kept constant across model scenario runs are given in Table SI-2. Model parameters that vary among the scenarios are given in Table SI-3.

SI-2.1 Mass and δ^{13}C conservation equations. The mass balances for organic (particulate and dissolved) and inorganic carbon are

$$\begin{aligned}\frac{dM_{\rm org}}{dt} &= F_{\rm prod} - F_{\rm remin} - F_{\rm b,org}\\ \frac{dM_{\rm inorg}}{dt} &= F_{\rm in} + F_{\rm remin} - F_{\rm prod} - F_{\rm b,inorg}\end{aligned} \qquad [\textbf{SI-1}]$$

Where $F_{\rm prod}$ is the rate of production of organic matter by oxygenic photosynthesis (in units of 10^{15}kg carbon per year), while $F_{\rm remin}$ is the remineralization by aerobic processes, and by sulfate reduction and iron reduction. $F_{\rm in}$ is the flux from volcanoes and weathering, and $F_{\rm b,org}$, $F_{\rm b,inorg}$ are the organic and inorganic burial rates. The mass balance equations for the fractions of organic and inorganic carbon that is of ^{13}C isotopic composition are,

$$\begin{aligned}\frac{d(\delta_{\rm org}M_{\rm org})}{dt} &= F_{\rm prod}(\delta_{\rm inorg}+\varepsilon) - F_{\rm remin}\delta_{\rm org} - F_{\rm b,org}\delta_{\rm org},\\ \frac{d(\delta_{\rm inorg}M_{\rm inorg})}{dt} &= F_{\rm in}\delta_{\rm in} + F_{\rm remin}\delta_{\rm org}\\ &\quad - F_{\rm prod}(\delta_{\rm inorg}+\varepsilon) - F_{\rm b,inorg}\delta_{\rm inorg}.\end{aligned} \qquad [\textbf{SI-2}]$$

The isotopic composition of new organic material is $\delta_{\rm inorg}+\varepsilon$, with $\varepsilon<0$. Using the above mass balance equations, the last two equations may be written as

$$\begin{aligned}M_{\rm org}\frac{d\delta_{\rm org}}{dt} &= F_{\rm prod}(\delta_{\rm inorg}+\varepsilon-\delta_{\rm org}),\\ M_{\rm inorg}\frac{d\delta_{\rm inorg}}{dt} &= F_{\rm in}(\delta_{\rm in}-\delta_{\rm inorg}) - (F_{\rm prod}-F_{\rm remin})\varepsilon\\ &\quad - F_{\rm remin}(\delta_{\rm inorg}+\varepsilon-\delta_{\rm org}).\end{aligned} \qquad [\textbf{SI-3}]$$

These are the equations used to obtain the model results discussed within the paper itself. Before proceeding with the model description, consider some further simplifications that are useful in order to get some intuition into the model results. Because of the large production and remineralization fluxes, the isotopic composition of organic matter, $\delta_{\rm org}$, tends to be in a quasi-steady state ($\frac{d}{dt}\delta_{\rm org}=0$), while the equations for the total organic and inorganic mass and the inorganic isotopic are not necessarily in a steady state. If the inorganic isotopic composition $\delta_{\rm inorg}$ undergoes an excursion, then at its minimum point, where $\frac{d}{dt}\delta_{\rm inorg}=0$ we have

$$\begin{aligned}\delta_{\rm org} &= \delta_{\rm inorg}+\varepsilon\\ \delta_{\rm inorg} &= \delta_{\rm in} - f^{\delta}\varepsilon,\end{aligned} \qquad [\textbf{SI-4}]$$

where

$$f^{\delta} = \frac{F_{\rm prod}-F_{\rm remin}}{F_{\rm in}} \qquad [\textbf{SI-5}]$$

Note that because a steady state is not assumed for the mass balance equations, f^{δ} is not necessarily equal to the organic burial fraction. The consequences of these relations are discussed in the accompanying paper.

Reserved for Publication Footnotes

SI-2.2 Increased export production and sulfate remineralization scenario. Following standard model formulation, we specify the background (that is, steady state values before the applied perturbation to the export production) remineralization and export production as fraction of the oxygenic production flux,

$$\begin{aligned} F_{\text{remin},0} &= \alpha_{\text{remin}} F_{\text{prod},0}, \\ F_{\text{ep},0} &= (1-\alpha_{\text{remin}}) F_{\text{prod},0}, \\ F_{\text{remin}} &= F_{\text{remin},\text{O}_2} + F_{\text{remin},\text{SO}_4} + F_{\text{remin},\text{Fe}}, \\ F_{\text{b,org}} &= F_{\text{ep},0}. \end{aligned} \qquad \textbf{[SI-6]}$$

Next, we specify the changes to the export production and remineralization fluxes during the enhanced export production scenario. With U the amplitude of the increase to the export production, we prescribe the changes to the oxygenic production and remineralization as well as to the anoxic remineralization by sulfate reduction and iron reduction, as fractions of U,

$$\begin{aligned} F_{\text{ep}} &= F_{\text{ep},0} + U F_{\text{ep},0} \mathcal{H}(t), \\ F_{\text{prod}} &= F_{\text{prod},0} - \gamma U F_{\text{ep},0} \mathcal{H}(t), \\ F_{\text{remin},\text{O}_2} &= F_{\text{remin},0} - \beta U F_{\text{ep},0} \mathcal{H}(t), \\ F_{\text{remin},\text{SO}_4} &= \alpha U F_{\text{ep},0} \mathcal{H}(t), \\ F_{\text{remin},\text{Fe}} &= \eta U F_{\text{ep},0} \mathcal{H}(t). \end{aligned} \qquad \textbf{[SI-7]}$$

The scaling factors α, β, γ and η are given in tables SI-2 and SI-3. The specified transient perturbation to the different carbon fluxes first increases and then decreases. The time dependence is a Gaussian in time, chosen for simplicity and represented by $\mathcal{H}(t) = \exp\left(-(t-t_0)^2/\tau_{\text{ep}}^2\right)$. Model experiments 7, 8 and 9 use instead a step-function like forcing having the same area under the curve,

$$\mathcal{H}(t) = \begin{cases} \sqrt{\pi}/2 & |t-t_0| < \tau_{\text{ep}} \\ 0 & \text{elsewhere} \end{cases} \qquad \textbf{[SI-8]}$$

which allows us to examine the model response time scale, please see discussion in section below. As seen in the accompanying paper, the perturbation to the fluxes leads to a CO_2 drawdown. One expects the ensuing glacial conditions to lead to a sever perturbation to the marine biology, so that the specified dependence of the fluxes beyond that point (i.e., the decaying part of the Gaussian perturbation) is not expected to be meaningful.

SI-2.3 The expanded carbonate system. The relevant set of dissociation and dissolution reactions is,

$$\begin{aligned} \text{CO}_2(\text{g}) &\rightleftharpoons \text{H}_2\text{CO}_3^* \\ \text{H}_2\text{O} &\rightleftharpoons \text{H}^+ + \text{OH}^- \\ \text{H}_2\text{CO}_3^* &\rightleftharpoons \text{H}^+ + \text{HCO}_3{}^- \\ \text{HCO}_3^- &\rightleftharpoons \text{H}^+ + \text{CO}_3{}^{-2} \\ \text{B(OH)}_3 + \text{H}_2 &\rightleftharpoons \text{H}^+ + \text{B(OH)}_4^- \\ \text{HSO}_4^- &\rightleftharpoons \text{H}^+ + \text{SO}_4^{2-} \\ \text{H}_2\text{S(aq)} &\rightleftharpoons \text{HS}^- + \text{H}^+ \end{aligned} \qquad \textbf{[SI-9]}$$

where $\text{H}_2\text{CO}_3^* \equiv \text{CO}_2^* \equiv \text{CO}_2(\text{aq}) + \text{H}_2\text{CO}_3$, and it is assumed that the first dissociation of the sulfuric acid, H_2SO_4, is complete because it is a strong acid. The 12 unknowns are,

$$\begin{aligned} &\text{H}^+, \text{OH}^-, \\ &\text{CO}_2(\text{g}), \text{H}_2\text{CO}_3^*, \text{HCO}_3^-, \text{CO}_3{}^{-2}, \\ &\text{B(OH)}_3, \text{B(OH)}_4^-, \\ &\text{HSO}_4^-, \text{SO}_4^{2-} \\ &\text{H}_2\text{S(aq)}, \text{HS}^-. \end{aligned} \qquad \textbf{[SI-10]}$$

These are solved for using the above 7 equations of the expanded carbonate system, plus 5 constraints on the total carbon, total boron, total sulfate, total sulfide and a generalized alkalinity Alk_G (all of which to be calculate later via prognostic equations),

$$\begin{aligned} C_T &= [\text{H}_2\text{CO}_3{}^*] + [\text{HCO}_3{}^-] + [\text{CO}_3{}^{-2}], \\ B_T &= [\text{B(OH)}_4^-] + [\text{B(OH)}_3], \\ S_T &= [\text{HSO}_4^-] + [\text{SO}_4^{2-}], \\ (\text{H}_2\text{S})_\text{T} &= [\text{H}_2\text{S(aq)}] + [\text{HS}^-], \\ Alk_G &= [\text{HCO}_3{}^-] + 2[\text{CO}_3{}^{-2}] + [\text{B(OH)}_4^-] + [\text{HSO}_4^-] \\ &\quad + 2[\text{SO}_4^{2-}] + [\text{HS}^-] + [\text{OH}^-] - [\text{H}^+]. \end{aligned} \qquad \textbf{[SI-11]}$$

We include SO_4^{2-} and HSO_4^- in the charge balance, although the second dissociation of sulfuric acid is sufficiently complete that it could be assumed to occur completely. The contribution of variations in these terms to the variations in the charge balance turns out to be small, of the order of that due to the hydrogen Ion.

SI-2.4 Dissolution and precipitation of bottom sediments. The changes in DIC concentration lead to corresponding changes to the carbonate (CO_3^{2-}) ion concentration, which may bring CaCO_3 to under or over saturation and lead to dissolution or deposition of CaCO_3 sediments. This, in turn, would affect both the total DIC and the alkalinity and as a result regulate the pH. The inorganic burial also includes siderite formation and may be formulated as follows [1],

$$\begin{aligned} F_{\text{b,inorg},\ell} &= \frac{[Alk_0]}{\tau_{\text{CaCO}_3}} \text{sign}(\Delta\Omega)(\Delta\Omega)^{4.5} + F_{\text{siderite}}, \\ \Delta\Omega &\equiv \frac{[CO_3^{2-}]}{[CO_3^{2-}]_{\text{sat}}} - 1. \end{aligned} \qquad \textbf{[SI-12]}$$

The subscript ℓ in $F_{\text{flux},\ell}$ is the flux F_{flux} measured in units of μ mole carbon per liter per year instead of Peta (10^{15}) kg carbon per year,

$$\begin{aligned} F_{\text{flux},\ell} &= F_{\text{flux}} \frac{10^{15} kg\ C}{\text{year}} \times \frac{1}{V_{\text{ocean}}} \text{liter}^{-1} \times 83.3\, 10^6 \frac{\mu \text{ mole } C}{kg\ C} \\ &= \left(F_{\text{flux}} \times f_{c/\ell}\right) \frac{\mu \text{ mole } C}{\text{liter} \times \text{year}} \end{aligned} \qquad \textbf{[SI-13]}$$

where $f_{c/\ell} = 60.8$.

SI-2.5 Weathering. Assume that a fraction $0 \le \alpha_{\text{wthr}} \le 1$ of the CO_2 from volcanic activity finds its way to the ocean via silicate weathering, while the rest, $1 - \alpha_{\text{wthr}}$, is absorbed by the ocean directly, without the accompanying Ca^{2+}. The weathering fraction α_{wthr} is a function of the temperature, as a higher temperature leads to enhanced chemical weathering.

We parameterize the dependence of α_{wthr} on temperature following Berner's GEOCARB II model (eqn 31 in [2]),

$$f_B(T) = \{\exp[0.090(T-T_0)]\} \times [1 + 0.038(T-T_0)]^{0.65}$$

where T_0 is the present-day global mean temperature. Prescribing a relation between temperature and atmospheric CO_2 we can write the above weathering feedback as function of CO_2 ([2] eqn 33, neglecting fertilization effects for land plants

which did not exist yet during the Neoproterozoic, as well as solar variations),

$$f_B(RCO_2) = (RCO_2)^{0.09\Gamma} \times [1 + 0.038\Gamma \ln(RCO_2)]^{0.65}$$

where RCO_2 is the ratio between the pCO_2 concentration and that of present day. The sensitivity of temperature to CO_2 is given by Γ which is defined via,

$$T(t) - T(0) = \Gamma \ln(RCO_2),$$

so that a value of $\Gamma = 6°C$ corresponds to a $4°C$ warming for a doubling of CO_2. The parameterization $f_B(RCO_2)$ is monotonically increasing as function of the pCO_2 and we set the weathering fraction to be,

$$\alpha_{\rm wthr}(RCO_2) = \alpha_{wthr,0} \times f_B(RCO_2). \qquad [\textbf{SI-14}]$$

This parameter is, of course, allowed to vary only between zero and one.

SI-2.6 Calcium ion budget. The concentration of Ca^{2+} depends on both the sedimentation rate and the input from weathering,

$$\frac{d}{dt}{\rm Ca}^{2+} = F_{{\rm in},{\rm Ca}^{2+},\ell} - F_{\rm b,inorg,\ell}, \qquad [\textbf{SI-15}]$$

Where $F_{{\rm in},{\rm Ca}^{2+},\ell}$ is a prescribed input flux (calculated using the weathering parameterization), and the second term represents the effect of sedimentation/dissolution on $CaCO_3$.

The calcium carbonate precipitation reaction may be written in several equivalent ways, all involving the loss of two alkalinity unit and one DIC unit. This has the net effect of increasing pCO_2 and, by itself, could function as a negative feedback on the scenario analyzed here. But this reaction needs to be considered together with the rest of the picture and in particular the burial of DIC via siderite formation and the addition of alkalinity via sulfat reduction followed by pyrite formation. With these processes included, the net effect presented in the scenario here is a reduction of atmospheric pCO_2.

SI-2.7 Remineralization via sulfate reduction. The anoxic remineralization of organic matter via sulfate (SO_4^{2-}) reduction, most likely occurring in the upper sediment layers, leads to the formation of sulfide (H_2S, or in dissociated form, HS^-) which can then either diffuse toward the oxygenated upper ocean and be oxidized there back into sulfate, or react with iron to form pyrite. These three processes may be represented by,

$$\begin{aligned} 2{\rm CH_2O} + {\rm SO_4^{2-}} &\rightarrow {\rm HS^-} + {\rm H_2O} + {\rm CO_2} + {\rm HCO_3^-}, \\ {\rm HS^-} + 2{\rm O_2} &\rightarrow {\rm SO_4^{2-}} + {\rm H^+}, \\ {\rm Fe^{2+}} + 2{\rm HS^-} &\rightarrow {\rm FeS_2} + {\rm H_2}. \end{aligned} \qquad [\textbf{SI-16}]$$

The oxidation of organic matter via sulfate reduction leads to a change in the sulfate and sulfide concentrations (as well as contributes to the mass and isotopic balances, see section SI-2.1) as follows,

$$\begin{aligned} \frac{d}{dt}({\rm H_2S})_T &= +\frac{1}{2}F_{{\rm remin},{\rm SO_4},\ell}, -F_{\rm H_2S,mixing} - F_{\rm pyrite}, \\ \frac{d}{dt}S_T &= -\frac{1}{2}F_{{\rm remin},{\rm SO_4},\ell} + F_{\rm H_2S,mixing}. \end{aligned} \qquad [\textbf{SI-17}]$$

The factor of one half is needed because the oxidation of two mole of carbon involves turning one mole of sulfate into H_2S. The mixing and pyrite formation fluxes are parameterized as,

$$\begin{aligned} F_{\rm H_2S,mixing} &= \frac{({\rm H_2S})_T}{\tau_{\rm mixing}}, \\ F_{\rm pyrite} &= \frac{({\rm H_2S})_T}{\tau_{\rm pyrite}}, \end{aligned} \qquad [\textbf{SI-18}]$$

where $\tau_{\rm mixing}$ and $\tau_{\rm pyrite}$ are specified time scales for both processes, and these fluxes are in units of moles of S per unit time. In the present-day ocean nearly all (about 90%) of the sulfide formed in the sediments by sulfate reduction escapes into the ocean and is oxidized there back to sulfate. In the anoxic Neoproterozoic ocean, one expects that even some of the sulfide escaping into the water column will still form pyrite there before getting to the oxygenated upper ocean. We therefore choose the pyrite formation time scale to be equal to the mixing time scale. As a result, half of the sulfide forms pyrite and half is oxidized. Changing this ratio does not have a significant effect on the results. If more of the sulfide is oxidized into sulfate, one needs to postulate more export production of organic matter to remineralized and contribute to the alkalinity budget and CO_2 reduction. The scenario is not significantly affected otherwise and, in particular, the total required sulfate or iron, the limiting factors in this scenario as explained in the paper, do not change. Finally, note that the pyrite formation [**SI-16**]c also affects the generalized alkalinity as defined here [**SI-11**] by removing sulfide ions HS^-.

SI-2.8 Remineralization via iron reduction. Next, consider the anoxic remineralization of the exported organic matter by iron reducing bacteria which reduce Fe^{3+} into Fe^{2+} while remineralizing the organic matter into DIC. This reaction may again be followed by either the mixing of Fe^{2+} to the upper ocean and its oxidation back into Fe^{3+}, or by siderite ($FeCO_3$) formation. These three reactions are represented by,

$$\begin{aligned} 2{\rm CH_2O} + 8{\rm Fe(OH)_3} &\rightarrow 8{\rm Fe^{2+}} + 2{\rm HCO_3^-} \\ &\quad + 14{\rm OH^-} + 6{\rm H_2O}, \\ 8{\rm Fe^{2+}} + 2{\rm O_2} + 20{\rm H_2O} &\rightarrow 8{\rm Fe(OH)_3} + 16{\rm H^+}, \\ 8{\rm Fe^{2+}} + 8{\rm CO_3^{2-}} &\rightarrow 8{\rm FeCO_3}. \end{aligned} \qquad [\textbf{SI-19}]$$

Fe^{2+} is soluble, and given the above stoichiometry we write an equation for its concentration, including the production by iron reduction, the loss to siderite formation and the gain from the oxidation of Fe^{3+} as follows,

$$\frac{d}{dt}{\rm Fe}^{2+} = 4F_{{\rm remin,Fe}}/f_{c/\ell} - F_{\rm siderite} - F_{\rm Fe,mixing}. \qquad [\textbf{SI-20}]$$

Fe^{3+} is practically insoluble, it accumulates in the sediments where it can be used by iron reducing bacteria [3,4]. We need to estimate the Fe^{3+} flux required to sustain the iron remineralization. The rate of consumption of Fe^{3+} (calculated initially for convenience in units of micromole per liter per year) is given by,

$$\frac{d}{dt}{\rm Fe}^{3+} = -4F_{{\rm remin,Fe}}/f_{c/\ell} + F_{\rm Fe,mixing}, \qquad [\textbf{SI-21}]$$

and the implied needed iron flux into the ocean in moles iron per year is then obtained by multiplying the left hand side by the ocean volume in liters and converting from micromoles to moles,

$${\rm Flux}({\rm Fe}^{3+}) = 10^{-6}V_{\rm ocean}\frac{d}{dt}{\rm Fe}^{3+}. \qquad [\textbf{SI-22}]$$

We parameterize the rate of siderite deposition in the sediments, as well as the rate of mixing of Fe^{2+} into the aerobic upper ocean zone, where it is oxidized back to Fe^{3+}, similarly

to the formulation of pyrite formation and sulfide oxidation in the previous subsection, in moles Fe per unit time, as,

$$F_{\text{siderite}} = \frac{Fe^{2+}}{\tau_{\text{siderite}}},$$
$$F_{\text{Fe,mixing}} = \frac{Fe^{2+}}{\tau_{\text{mixing}}}. \qquad \textbf{[SI-23]}$$

It is worth noting that the siderite formation reaction appears in the literature in different forms. Some of these, including the one used here, are,

$$Fe^{2+} + CO_3^{2-} \rightarrow FeCO_3,$$
$$Fe^{2+} + HCO_3^- + OH^- \rightarrow FeCO_3 + H_2O,$$
$$Fe^{2+} + 2HCO_3^- \rightarrow FeCO_3 + CO_2 + H_2O.$$

While these are different reactions, it is important to note that they are completely equivalent from our perspective here. All involve the loss of two units of alkalinity (either as CO_3^{2-}, $2HCO_3^-$, or a combination of HCO_3^- and OH^-). All three also involve the net loss of one unit of DIC (in the third reaction two units are lost on the left hand side, but one is gained back on the rhs).

CO_2, HCO_3^- and OH^- are all in equilibrium within the ocean carbonate system. Because the above three siderite formation reactions have the same effects on DIC and alkalinity, and because we equilibrate the carbonate system at every time step of the model, the three are completely equivalent and would lead to the same changes to the pH and pCO_2.

SI-2.9 Alkalinity budget. The weathering flux of each mole of carbon in the form of $CaCO_3$ is accompanied by a two mole change in alkalinity due to the double charge of CO_3^{2-}. In addition, the alkalinity budget is affected by the inorganic burial of calcium carbonate which removes carbonate ions, pyrite formation eliminates sulfide ions, siderite formation eliminates carbonate ions again, and iron reduction and oxidation also affect the alkalinity as discussed above. The corresponding alkalinity budget equation is therefore,

$$\frac{d}{dt}Alk_G = 2 \times \alpha_{\text{wthr}} F_{in,\ell} - 2 \times F_{\text{b,inorg},\ell} - F_{\text{pyrite}} + 8F_{\text{remin,Fe}} - 2F_{\text{Fe,mixing}} - 2F_{\text{siderite}}. \qquad \textbf{[SI-24]}$$

Note that two moles of alkalinity are lost per mole of iron deposited as siderite **[SI-19]**c, two moles of alkalinity are lost per mole of Fe^{2+} diffusing toward the aerobic zone and being oxidized to Fe^{3+}, while 8 moles of alkalinity are gained per mole of carbon remineralized by iron reduction **[SI-19]**a. Also remember that F_{pyrite} is in units of moles of S per unit time rather than moles of pyrite buried per unit time.

SI-2.10 Solving the expanded carbonate system. In the first subsection below (SI-2.10.1) we describe the numerical algorithm for solving the full expanded carbonate system, as used in the model solutions presented above. The standard method of forming a polynomial equation and solving it iteratively is not appropriate in this case given the larger number of equations which leads to a high order polynomial. We therefore use a gradient based optimization method and provide the gradient analytically. The second subsection (SI-2.10.2) describes the solution of an approximate carbonate system which includes sulfide, yet is sufficiently simple to provide some intuition into the full solution.

SI-2.10.1 Numerical solution of the full expanded carbonate system

In order to solve the carbonate system using an optimization approach, write the equations for the dissociation reactions **[SI-9]** as,

$$K_w = [H^+][OH^-],$$
$$K_0(T,S,P) = \frac{[H_2CO_3^*]}{[CO_2(g)]},$$
$$K_1(T,S,P) = \frac{[H^+][HCO_3^-]}{[H_2CO_3^*]},$$
$$K_2(T,S,P) = \frac{[H^+][CO_3^{-2}]}{[HCO_3^-]},$$
$$K_{HSO_4} = \frac{[H^+][SO_4^{2-}]}{[HSO_4^-]},$$
$$K_B = \frac{[H^+][B(OH)_4^-]}{[B(OH)_3]},$$
$$K_{H_2S,1}(T,S,P) = \frac{[H^+][HS^-]}{[H_2S(aq)]}. \qquad \textbf{[SI-25]}$$

Where the carbonate dissociation constants are taken from [5]. Sulfate and sulfide dissociation constants are from from "AquaEnv" [6]. We take $pH = -\log_{10}([H+])$. Differences from other scales should be minor. Together with the definitions of total carbon, sulfate, sulfide, boron and alkalinity **[SI-11]**, we write the complete set of equations in the following form,

$$0 = F_1 = K_w - [H^+][OH^-]$$
$$0 = F_2 = K_0(T,S,P)[CO_2(g)] - [H_2CO_3^*]$$
$$0 = F_3 = K_1(T,S,P)[H_2CO_3^*] - [H^+][HCO_3^-]$$
$$0 = F_4 = K_2(T,S,P)[HCO_3^-] - [H^+][CO_3^{-2}]$$
$$0 = F_5 = K_{HSO_4}[HSO_4^-] - [H^+][SO_4^{2-}]$$
$$0 = F_6 = K_B[B(OH)_3] - [H^+][B(OH)_4^-]$$
$$0 = F_7 = K_{H_2S,1}[H_2S(aq)] - [H^+][HS^-]$$
$$0 = F_8 = [H_2CO_3{}^*] + [HCO_3{}^-] + [CO_3{}^{-2}] - C_T$$
$$0 = F_9 = [B(OH)_4^-] + [B(OH)_3] - B_T$$
$$0 = F_{10} = [HSO_4^-] + [SO_4^{2-}] - S_T$$
$$0 = F_{11} = [HS^-] + [H_2S(aq)] - (H_2S)_T$$
$$0 = F_{12} = [HCO_3{}^-] + 2[CO_3{}^{-2}] + [B(OH)_4^-] + [HSO_4^-] + 2[SO_4^{2-}] + [HS^-] + [OH^-] - [H^+] - Alk_G$$

Ordering the vector of unknowns as shown in Table SI-1, the Jacobian (needed for the optimization solver) is,

$$\frac{\partial F_i}{\partial X_j} = \begin{pmatrix} \frac{\partial F_1}{\partial X_1} & \cdots & \frac{\partial F_1}{\partial X_n} \\ \frac{\partial F_2}{\partial X_1} & \cdots & \frac{\partial F_2}{\partial X_n} \\ & \ddots & \\ \frac{\partial F_n}{\partial X_1} & \cdots & \frac{\partial F_n}{\partial X_n} \end{pmatrix} \qquad \textbf{[SI-26]}$$

which, for the above system is again shown in Table SI-1.

For the optimization routine to work efficiently, we scale the variables and Jacobian to make all variables order one,

$$X_i' = X_i/\text{scale}_i,$$
$$\frac{\partial F_i}{\partial X_j'} = \text{scale}_j \frac{\partial F_i}{\partial X_j}.$$

We use Matlab's fsolve routine and the resulting solution of the expanded carbonate system is accurate to round-off error.

SI-2.10.2 Approximate solution of the expanded carbonate system

Consider an approximate solution to the carbonate+sulfide system. The approximation used here for DIC is valid only at pH values around 8, and for small perturbations to the DIC and H_2S. It is not used in the model calculations and is only shown in order to provide intuition into the expanded carbonate system.

Let the unknowns be the concentrations of $CO_2(g)$, $CO_2(aq)$, HCO_3^-, CO_3^{2-}, $H_2S(aq)$, HS^-, H^+. With a total of seven unknown, we need seven equations,

$$\begin{aligned} K_H &= \frac{[CO_2(aq)]}{[CO_2(g)]}, \\ K_1 &= \frac{[HCO_3^-][H^+]}{[CO_2(aq)]}, \\ K_2 &= \frac{[CO_3^{2-}][H^+]}{[HCO_3^-]}, \\ K_{S1} &= \frac{[HS^-][H^+]}{[H_2S(aq)]}, \\ C_T &= [HCO_3^-] + [CO_3^{2-}], \\ (H_2S)_T &= [HS^-] + [H_2S(aq)] \approx [HS^-], \\ Alk &= [HCO_3^-] + 2[CO_3^{2-}] + [HS^-]. \end{aligned} \qquad \textbf{[SI-27]}$$

The last three equations give,

$$\begin{aligned} [HCO_3^-] &= 2C_T - [Alk - (H_2S)_T] = 2C_T - Alk_C, \\ [CO_3^{2-}] &= [Alk - (H_2S)_T] - C_T = Alk_C - C_T, \\ [HS^-] &= (H_2S)_T, \end{aligned}$$

where the carbonate alkalinity is given by

$$Alk_C \equiv [HCO_3^-] + 2[CO_3^{2-}] = Alk - HS^- \approx Alk - (H_2S)_T.$$

Using the K_2 equation,

$$[H^+] = K_2 \frac{2C_T - Alk_C}{Alk_C - C_T},$$

next, using the K_1 equation,

$$[CO_2(aq)] = \frac{K_2}{K_1} \frac{(2C_T - Alk_C)^2}{Alk_C - C_T}$$

which, using Henry's law, gives

$$[CO_2(g)] = \frac{K_2}{K_1 K_H} \frac{(2C_T - Alk_C)^2}{Alk_C - C_T}. \qquad \textbf{[SI-28]}$$

Given that $Alk_C > C_T$, the last equation makes it clear that if the carbonate alkalinity increases, the atmospheric CO_2 decreases.

SI-3. Pyrite formation

Pyrite, FeS_2, is believed to commonly form in anoxic marine sediments via a reaction of Fe^{2+} with sulfide H_2S resulting from sulfate reduction of organic matter. The formation proceeds in two stages. The first phase [7] is the formation of brownish black amorphous Fe^{2+} monosulfide, FeS,

$$Fe^{2+} + HS^- \rightarrow FeS_{(s)} + H^+, \qquad \textbf{[SI-29]}$$

which, according to [7], is actually a shorthand for,

$$[Fe(H_2O)_6]^{2+} + HS^- \rightarrow FeS_{(s)} + H^+ + 6H_2O.$$

The iron monosulfide can take several forms and have different stoichiometric relations around F_1S_1. When it forms crystals it is exactly represented by FeS with a small (nano scale) crystal size, and is then referred to as Mackinawite [7], although this name is used for non-crystalline amorphous iron monosulfide by some authors.

The literature contains several possible scenarios and some strong disagreements regarding the second phase of pyrite formation. Some [8–10] suggest that this occurs via oxidation by elemental sulfur,

$$FeS + S^0 \rightarrow FeS_2 \qquad \textbf{[SI-30]}$$

This requires a reaction for the formation of S^0 from H_2S, probably via some bacterial path [9, 10]. However, [7] point out that S^0 is in fact S_8, making the above reaction an impossible multi-molecular reaction step mechanism, although the stoichiometry of the reaction may still be correct.

Alternatively, the second step may occur via an oxidation by H_2S,

$$FeS + H_2S \rightarrow FeS_2 + H_{2(g)} \qquad \textbf{[SI-31]}$$

In this case the combined pyrite formation reaction of **[SI-29]** and **[SI-31]** is

$$Fe^{2+} + HS^- + H_2S \rightarrow FeS_2 + H_{2(g)} + H^+$$

which is stoichiometrically equivalent to

$$Fe^{2+} + 2HS^- \rightarrow FeS_2 + H_{2(g)}. \qquad \textbf{[SI-32]}$$

This is the reaction used in the paper itself and it is further justified below.

Interestingly, [8] states that reaction **[SI-32]** "has never been observed ... during several years of experimentation". [11] do observe the reaction **[SI-32]** at 100°C, yet [12] reject the scenario of **[SI-31]** and **[SI-32]**, present experimental data showing that as long as the iron monosulfide is kept in a reducing atmosphere, devoid of any reactant other than H_2S, Mackinawite is the stable phase and the formation of pyrite is inhibited. They state,

> Numerous experimental studies have demonstrated that at temperatures below 100°C the conversion of unoxidized Mackinawite to pyrite is a very slow process. It was shown that this is not an important process in low temperature pyrite formation ...

and

> These new experiments have shown that in reducing H_2S and HS^- solutions, pyrite forms at a negligible to very slow rate.

The very extensive review by [7] suggests how to resolve these contradicting results. They, and [13], first explain that the conversion of monosulfide (Mackinawite or otherwise) to pyrite is not a solid phase reaction. The oxidation of FeS to pyrite involves the dissolution of FeS to form an aqueous FeS complex, FeS(aq), which is oxidized to form FeS_2, which is then recrystallized as pyrite. During this process, the S(-II) is oxidized to S(-I) and the Fe^{2+} remains unoxidized. As an evidence that this cannot be a solid phase reaction they show that the formed crystals of pyrite are orders of magnitude larger than the original ones of Mackinawite. In this sense solid Mackinawite is not strictly a necessary precursor for pyrite formation.

According to [7], pyrite formation involves two distinct physical processes, nucleation and crystal growth. Pyrite crystal growth is quite fast, but nucleation of pyrite crystals is slow and can be the rate-limiting phase in the conversion of

monosulfide to pyrite. The critical point is that the nucleation is sensitive to trace element catalysis and inhibitors. As an example of such catalytic effects on the formation of iron sulfides, [13] demonstrate the catalytic effect of aldehydic carbonyl groups (-CHO) in the formation of greigite, Fe_3S_4, from amorphous FeS via the H_2S path.

In a related paper, [14] demonstrate the sulfide path **[SI-29]**, **[SI-31]** and **[SI-32]** under strictly anoxic conditions. They also explain that,

> The metastable persistence of FeS with H_2S is well known [12, 15]. The pyrite nucleation barrier must be overcome for bulk formation of FeS_2, since pyrite formation on a suitable substrate with only FeS and H_2S is fast [16]. Such substrates are reaction initiators and may include partially oxidized FeS [12], greigite, sulfur grains, bacterial cell walls [17] or pyrite [16].

The role of bacterial cell walls was demonstrated by [17] who write "In vitro enrichment cultures of dissimilatory sulfate-reducing bacteria precipitated FeS and catalyzed its transformation into FeS_2 at ambient temperature and pressure under anaerobic conditions. When compared to purely abiotic processes, the bacterially mediated transformation was shown to be more efficient in transforming FeS into FeS_2."

It is important to realize that some alternative pyrite formation scenarios such as SI-30 and some others considered in the litetarute lead to the elimination of alkalinity added during sulfate reduction, and eliminate the pCO_2 reduction predicted here. While pyrite formation is not sufficiently well understood to rule out the path used here, we do note that this issue adds uncertainty to our proposed scenario of pCO_2 reduction via sulfate remineralization.

The bottom line is that in the presence of appropriate catalysts, especially organic materials of which there should be no shortage in anoxic sediments where pyrite forms, the H_2S path **[SI-32]** seems an appropriate representation of pyrite formation. The reason this path was not seen in many experiments is most likely that they were conducted under inorganic conditions and without the needed catalysts to accelerate the rate-limiting nucleation phase of pyrite formation. Even if one does not accept the catalyst scenario, the debate in the literature indicates that **[SI-32]** is considered at least by some a possible path for pyrite formation, and one is justified in considering its consequences as we do here.

SI-3.1 The fate of hydrogen from pyrite formation. The hydrogen produced by the pyrite formation in the anoxic sediments **[SI-32]** may be used by methanogens,

$$4H_2 + CO_2 \rightarrow CH_4 + 2H_2O. \qquad \textbf{[SI-33]}$$

Some of the methane may accumulate in the deep ocean as methane clathrates and this reaction can therefore contribute to the reduction of the total DIC. Alternatively, some of the methane could diffuse up to the oxic upper ocean to be oxidized back to CO_2,

$$CH_4 + 2O_2 \rightarrow CO2 + 2H_2O. \qquad \textbf{[SI-34]}$$

The net reaction is therefore simply

$$4H_2 + 2O_2 \rightarrow 2H_2O, \qquad \textbf{[SI-35]}$$

and may be ignored as far as the effect on alkalinity or total CO_2.

It is interesting to note that the above path leading to the accumulation of methane clathrates could be linked to the snowball initiation scenario of [18] if these clathrates are released to the atmosphere at some later time.

SI-4. Additional scenarios and sensitivity study

The parameters for the different scenarios shown here and in the main paper are all given in Tables SI-2 and SI-3. Fig. SI-1 shows fuller details of scenario #1 from the main paper, were aerobic remineralization is used to produce an isotopic signal of 15 permil and results in a very large pCO_2 increase.

SI-4.1. Additional scenarios. Figs. SI-3 and SI-4 show scenarios #3 and #4 in which the same isotopic signal and pCO_2 decrease presented in our main scenario (#2, Fig. 3 in the paper) are obtain by sulfate reduction only and by iron reduction only, correspondingly. Note the larger requirements of sulfate and Fe^{3+} in these two scenarios, correspondingly.

Scenario #5 (Fig. SI-5) shows the same isotopic signal, but effectively no change in atmospheric CO_2. Finally, Fig. SI-6 shows the results of scenario #6 in which the same CO_2 drawdown is obtained as in our main scenario (#2, Fig. 3 in paper), but with no isotopic signal. Note that hardly any net remineralization is needed in this case.

While also being interesting on their own, taken together, these scenarios compose a set of sensitivity experiments. These experiments, together with the corresponding model parameter values in Table SI-3, demonstrate that the scenarios leading to an isotopic signal as well as a CO_2 reduction are not overly sensitive to the model assumptions and occur over a robust regime of the model parameter space. However, we also perform an explicit sensitivity study of specific major parameters, as described in the following subsection.

SI-4.2. Sensitivity study. The set of sensitivity model experiments is summarized in Table SI-3.

Scenarios 7, 8 and 9 (Figs. SI-7, SI-8, SI-9) repeat the sequence of 2, 3 and 4 (both sulfate and iron reduction, sulfate only and iron only, correspondingly), but the temporal structure of the forcing is prescribed to be step-like instead of Gaussian. This has the important advantage of not focing a time scale on the model and allowing it to observe the model response time scales. The step-like forcing has exactly the same net effect as the Gaussian perturbations (see discussion of equation **[SI-8]** above). The first obvious conclusion from this experiment is that the amplitude of the response does not depend on the time structure of the forcing. See Figs. SI-2 and SI-7 for the remarkably similar amplitudes of DIC (panel c), isotopic signal (panel c), pH and atmospheric CO_2 (panel i), for example. Next, these experiments show which time dependence of the model is a result of the specified structure of the forcing and which is inherent to the model. For example, the DIC and isotopic signal clearly react to the forcing structure, while the pCO_2 and pH respond on the time scale of the carbonate system determined mostly by the time scale of the reaction with the bottom sediments (we assume the ocean and atmosphere to be in instantaneous equilibrium, not resolving the time scale of thousands of years involved with this equilibration).

Scenarios 10 and 11 perturb the climate sensitivity Γ from its value used in the original Berner model of 4 degree C per doubling of CO_2 to 5 and 3 degrees, correspondingly. The results are shown in Figs. SI-10 and SI-11, and are not overly sensitive to this parameter. Overall, silicate weathering provides a negative climate feedback: a reduction of atmospheric CO_2 leads to cooling, slowing of silicate weathering reactions and therefore the delivery of alkalinity to the ocean, and thus a decrease in the rate of CO_2 removal via carbonate precipitation. Larger climate sensitivity Γ (scenario 10) leads to stronger reduction of the minimum weathering fraction value,

to $\alpha_{\rm wthr} = 0.53$ at the peak of the event, to a smaller alkalinity flux and therefore to a smaller corresponding CO_2 reduction, to 174 ppm. A smaller climate sensitivity (scenario 11) leads to a smaller reduction of the weathering fraction of $\alpha_{\rm wthr} = 0.55$, to a larger alkalinity flux, and a corresponding CO_2 reduction to 134 ppm.

The parameters α, β and γ control the amplitude of perturbations to the sulfate reduction remineralization, aerobic remineralization and oxygenic production, correspondingly (SI-7). These parameters are selected in the above scenarios to obtain results which seem interesting, yet their values are clearly somewhat arbitrary in our scenarios and therefore it is important to study their sensitivity, as is done in scenarios 12-17. The runs are summarized in Table SI-3 and shown in Figs. SI-12, SI-13, SI-14, SI-15, SI-16 and SI-17.

The change in the specified reduction in oxygenic production, controlled by γ, between experiments 16 and 17 is quite significant, about 25%. In response, the corresponding CO_2 reduction is to 100ppm in one case and to 200ppm in the other (compare scenarios 16 and 17, Figs. SI-16i and SI-17i). So while this parameter affects the results, they are clearly not overly sensitive to its value.

A change of about 30% in the sulfate remineralization rate factor α, from 0.7 to 0.9, leads from a CO_2 decrease of some 200ppm, to an increase of about 100ppm (compare scenarios 12 and 13, Figs. SI-12i and SI-13i). This seems a sizable change, but is negligible relative to the CO_2 increase to 60,000ppm when no anaerobic remineralization is used (scenario 1). The model is also not overly sensitive to the aerobic remineralization rate factor, β (compare scenarios 12 and 13, Figs. SI-14i and SI-15i).

SI-5. Consequences to oxygen cycle

The oxygenic fixing of organic matter, balanced by anaerobic remineralization, leads to the accumulation of oxygen in the ocean and atmosphere. On the other hand, the consumption of oxygen via sulfide oxidation and iron oxidation leads to the loss of oxygen. Consider an estimate of the magnitude of these effect and their consequences.

Begin with the oxygen production rate. The net perturbation to the aerobic remineralization and oxygenic production rates is given by (in gr C/year) $F_{\rm net\,C}(t) = \Delta F_{\rm prod}(t) - \Delta F_{\rm remin}(t)$, where $\Delta F_{\rm prod}(t) = F_{\rm prod}(t) - F_{\rm prod}(0)$. These carbon fluxes involved in the production of oxygen are shown in Fig. SI-18a. Each net mole of fixed organic carbon leads to the production of one mole of O_2, so that the implied oxygen flux into the ocean and atmosphere, in moles O_2 per year, is $F_{\rm O_2}(t) = F_{\rm net\,C}(t)/12$, shown by the green line in Fig. SI-18b.

Next, let us address the consumption of oxygen in the scenario examined here. The two relevant reactions are those representing sulfide and iron oxidation,

$$\mathrm{HS^- + 2O_2 \rightarrow SO_4^{2-} + H^+},$$
$$\mathrm{8Fe^{2+} + 2O_2 + 20H_2O \rightarrow 8Fe(OH)_3 + 16H^+}.$$

Thus oxidizing of one mole of sulfide ion involves the loss of two moles of O_2, while the oxidation of eight moles of Fe^{2+} also leads to the loss of two moles of O_2.

Combining the above oxygen sources and sinks, we can write the rate of change of oxygen (moles per liter per unit time) as follows,

$$\frac{d\mathrm{O_2}}{dt} = \frac{1}{12}F_{\rm net\,C}(t) - \frac{2}{8}F_{\rm Fe,mixing} - 2F_{\rm H_2S,mixing} \quad \textbf{[SI-36]}$$

Note that $F_{\rm Fe,mixing}$ is in units of moles Fe^{2+} per unit time, while $F_{\rm H_2S,mixing}$ is in units of moles S per unit time. The sources and sinks sinks for oxygen are shown in Fig. SI-18b.

Combining these effects together, Fig. SI-18c shows the net oxygen production rate (source minus sinks) during the scenario. To maintain the oxygen concentration unperturbed, this flux would need to be balanced by sinks such as the O_2 sink due to weathering flux, estimated at present at about 15×10^{12} moles O_2 per year [19] and shown as the green dashed line in Fig. SI-18c. The implied net oxygen source $F_{\rm O_2}(t)$ and the weathering flux seem to be of similar magnitudes, suggesting that the weathering flux and other sinks may have been able to regulate the oxygen level during the scenario. However, we need to remember that the weathering flux before the advent of land plants could have been as much as one order of magnitude weaker.

The implied oxygen source is therefore a non negligible addition to the ocean-atmosphere oxygen pool. If this leads to a significant rise in the atmospheric oxygen level, then the ocean anoxia may be reduced, affecting the assumptions behind the scenario considered here. The mechanisms maintaining the atmospheric oxygen concentration are not completely understood [19], and it is difficult to estimate therefore how efficient they would be in keeping the oxygen level down during such an injection of oxygen into the ocean and atmosphere. All we can currently do is point out this significant potential difficulty with the scenario examined here.

The ideas discussed here may be relevant to the suggestion of [20] that a pre-snowball drawdown of atmospheric oxygen into the ocean, leading to DOM oxidation and therefore to atmospheric pCO_2 increase, may help stabilize a slushball and prevent a hard snowball. We note that if the remineralization occurs via anaerobic processes as discussed here, followed by pyrite and siderite formation, this may lead to a drawdown of atmospheric pCO_2 instead.

SI-6. Sanity checks

The following order-of-magnitude checks on the results of the model help obtain some additional insight into the quantitative calculations and workings of the model, and serve as an additional check on the model results. Unless noted otherwise, we base these calculation on scenario #7 with step-like forcing, for which it is simpler to estimate the total perturbation to the forcing and the amplitude of the response, and compare to the shown results of the time dependent model calculations. All values used for the calculations below can be obtained from the shown Figures.

- Is the change in DOC consistent with the prescribed fluxes? The perturbations in aerobic remineralization, oxygenic production, sulfate reduction and iron reduction sum to a net remineralization rate of 1.6e-4-6.38e-4+1.1e-4+6.38e-4=2.7e-4 peta kg/yr for 0.604e6yr, and should lead to a 2.7e-4×1e15 kg C/yr×0.604e6yr=160e+15 kg C change in DOC, consistent with Fig. SI-7c.
- Is the isotopic signal consistent with the amount of DOC remineralized? Given the initial (δ_0) and final (δ_1) isotopic concentrations, we can write the isotopic mass balance for ^{13}C as,
$$200(DOC)\times\delta_0 + 50(DIC)\times(\delta_0 + 28)$$
$$= 50(DOC)\times\delta_1 + 200(DIC)\times(\delta_1 + 28)$$
which gives a change in the isotopic composition of $\delta_0 - \delta_1 = 16$, again consistent with Fig. SI-7c.
- Charge balance/ alkalinity: turning off the weathering feedback, dissolution and precipitation of calcium carbonate, and pyrite and siderite deposition, we verify that the

charge added via sulfate reduction is exactly balanced by changes to the carbonate, boron and sulfide charge concentration changes (Figure not shown, see scenario 18 in code files distributed with SI).

- DIC units: panel (b) of Fig 3 in the paper shows an increase in DIC concentration to be 0.208 mmole/liter (from 2.213 mmole/liter before the perturbation to 2.421 after the perturbation; the increase in the new equilibrium is due to the elimination of some of the Calcium). Panel (c) shows the increase in the total DIC to be 3.42 peta kg (from 36.38 peta kg to 39.80 peta kg). Multiplying the concentration by the ocean volume 13.7e20 liter and then by 12e-6 kg C/mmole, we see that the two diagnostics represent the same increase.
- How much oxygen is produced?
  In scenario 7, oxygenic production of organic matter decreases during the event by (0.0036-0.00344)=1.6e-4 peta kg/yr; aerobic remin decreased by a larger amount of (0.003564-0.002926)=6.38e-4 peta kg/yr. Net addition to oxygenic production is therefore 4.78e-4 peta kg/yr. The perturbation lasts (1.801-1.197)=0.604 Myr, so the implied accumulated carbon is (4.78e-4 peta kg/yr)×(0.604e6 yr)=2.887e17 kg C, which is equal to (2.887e20 g C)/(12 g C/mole)=2.4e19 mole C. Each mole of produced organic carbon leads to the production of one mole of O_2, so we have a net O_2 production: 2.4e19 mole O_2, or a production rate of 4e13 mole O_2/yr.
  However, as discussed in section below, oxygen is also consumed by Fe^{2+} and H_2S oxidation. Consider these fluxes next. The time scales for pyrite formation and sulfide oxidation are the same, so that half of the sulfide formed via sulfate reduction is oxidized (see $\tau_{\rm pyrite}$ and $\tau_{\rm mixing}$ in Table SI-2). Similarly, the time scales for siderite formation and Fe^{2+} oxidation are the same, so that half of the Fe^{2+} produced by iron reduction is oxidized (see $\tau_{\rm siderite}$ and $\tau_{\rm mixing}$ in Table SI-2).

  First, calculate the oxygen sink due to iron remineralization. The perturbation to iron remineralization via reduction is 0.003036-0.002926=1.1e-4 peta kg/yr, which amounts to (1.1e-1 peta g C/yr)/(12 g C/mole C)=9.17e12 mole C/year. Now, 4 moles of Fe^{2+} are produced per one mole of remineralized organic carbon (SI-19), so the above amounts to 36.68e12 mole Fe(II)/year. Half of this is oxidized, and each oxidized mole of Fe(II) consumes 0.25 mole of O_2 (SI-19), so we expect the O_2 consumption rate to be 36.68e12×0.5×0.25=4.585e12 moles O2/year, and over the perturbation period, this results in an Fe sink of (4.585e12 moles O_2/year)×(0.604e6 yr)=2.77e18 mole O_2.
  Next, calculate the oxygen sink due to sulfide oxidation. The perturbation to remineralization via sulfate reduction is 0.003564-0.002926=6.38e-4 peta kg/yr, which amounts to (6.38e-1 peta g/yr)/(12 g C/mole C)=5.32e+13 mole C/year. Now, half a mole of sulfide ion HS^- is produced per mole of remineralized carbon (SI-16) so the above sulfate reduction rate amounts to the production of 2.66e13 mole HS^-/year. Half of this is oxidized, and each oxidized mole of HS^- requires two moles of O_2, so we expect the O_2 consumption rate to be (2.66e13 mole HS^-/year)×0.5×2=2.66e13 mole O_2/year. Over the time of the perturbation, this should lead to an O_2 sink: S_{H_2S} =(2.66e13 mole O_2/year)×(0.604e6 yr)=1.61e+19 mole O_2.
  The total net production of O_2 is therefore $Source - S_{H_2S} - S_{Fe} = 2.4e19 - 2.77e18 - 1.61e19 = 5.13e18$ mole O_2 over a period of 0.604 Myr, or a rate of 8.5e12 mole O_2/year. These need to be compared with the present-day atmospheric content of oxygen, about 3e19 moles, and with the present-day sink of O_2 due to weathering and volcanoes of 1.5e13 mole O_2/year. The similarity of the flux of produced oxygen and of the oxygen sink makes it not implausible that this source flux could be regulated by the sink to keep oxygen concentration at a low value.

1. Berelson WM, Hammond DE, McManus J, Kilgore TE (1994) Dissolution kinetics of calcium carbonate in equatorial pacific sediments. Global Biogeochem. Cycles 8:219–235.
2. Berner R (1994) GEOCARB-II - a revised model of atmospheric CO_2 over Phanerozoic time. American Journal of Science 294:56–91.
3. Dong H, Jaisi DP, Kim J, Zhang G (2009) Microbe-clay mineral interactions. American Mineralogist 94:1505–1519.
4. Kostka J, Haefele E, Viehweger R, Stucki J (1999) Respiration and dissolution of iron(iii) containing clay minerals by bacteria. Environmental Science & Technology 33:3127–3133.
5. Zeebe R, Wolf-Gladrow D (2001) CO_2 in seawater: equilibrium, kinetics, isotopoes, Elsevier Oceanography Series (Elsevier) Vol. 65.
6. Hofmann AF, Soetaert K, Middelburg JJ, Meysman FJR (2010) AquaEnv - an aquatic acid-base modelling environment in R. Aquatic Geochemistry DOI 10.1007/s10498-009-9084-1.
7. Rickard D, Luther, III GW (2007) Chemistry of iron sulfides. Chemical Reviews 107:514–562.
8. Berner RA (1970) Sedimentary pyrite formation. American Journal of Science 268:1–23.
9. Berner R (1972) Sulfate reduction, pyrite formation, and the oceanic sulfur budget (Wiley Interscience division of John Wiley and sons, Inc), pp 347–361.
10. Berner RA (1984) Sedimentary pyrite formation - an update. Geochimica et Cosmochimica Acta 48:605–615.
11. Drobner E, Huber H, Wachtershauser G, Rose D, Stetter KO (1990) Pyrite formation linked with hydrogen evolution under anaerobic conditions. Nature 346:742–744.
12. Benning LG, Wilkin RT, Barnes HL (2000) Reaction pathways in the Fe-S system below 100 degrees C. Chemical Geology 167:25–51.
13. Rickard D, Butler I, Oldroyd A (2001) A novel iron sulphide mineral switch and its implications for earth and planetary science. Earth and Planetary Science Letters 189:85–91.
14. Butler I, Bottcher M, Rickard D, Oldroyd A (2004) Sulfur isotope partitioning during experimental formation of pynite via the polysulfide and hydrogen sulfide pathways: implications for the interpretation of sedimentary and hydrothermal pyrite isotope records. Earth and Planetary Science Letters 228:495–509.
15. Rickard D (1969) The chemistry of iron sulfide formation at low temperatures. Stockholm Contrib. Geol. 20:67–95.
16. Harmandas N, Fernandez E, Koutsoukos P (1998) Crystal growth of pyrite in aqueous solutions. inhibition by organophosphorus compounds. Langmuir 14:1250–1255.
17. Donald R, Southam G (1999) Low temperature anaerobic bacterial diagenesis of ferrous monosulfide to pyrite. Geochimica et Cosmochimica Acta 63:2019–2023.
18. Schrag DP, Berner RA, Hoffman PF, Halverson GP (2002) On the initiation of a snowball Earth. Geochemistry Geophysics Geosystems 3.
19. Catling DC, Claire MW (2005) How Earth's atmosphere evolved to an oxic state: A status report. Earth Planet. Sci. Lett. 237:1–20.
20. Peltier WR, Liu Y, Crowley JW (2007) Snowball earth prevention by dissolved organic carbon remineralization. Nature 450:813–U1.

Table SI-1. Order of variables of the expanded carbonate system, and the Jacobian [SI-26] for solving it.

$$X = \begin{bmatrix} H^+ & OH^- & CO_2(g) & H_2CO_3^* & HCO_3^- & {CO_3}^{-2} & B(OH)_3 & B(OH)_4^- \\ 1 & 2 & 3 & 4 & 5 & 6 & 7 & 8 \\ HSO_4^- & SO_4^{2-} & H_2S(aq) & HS^- & & & & \\ 9 & 10 & 11 & 12 & & & & \end{bmatrix}$$

$$\left\{\frac{\partial F_i}{\partial X_j}\right\} = \begin{pmatrix} -OH^- & -H^+ & 0 & 0 & 0 & 0 & 0 & 0 & 0 & 0 & 0 & 0 \\ 0 & 0 & K_0 & -1 & 0 & 0 & 0 & 0 & 0 & 0 & 0 & 0 \\ -HCO_3^- & 0 & 0 & K_1 & -H^+ & 0 & 0 & 0 & 0 & 0 & 0 & 0 \\ -CO_3^{2-} & 0 & 0 & 0 & K_2 & -H^+ & 0 & 0 & 0 & 0 & 0 & 0 \\ -SO_4^{2-} & 0 & 0 & 0 & 0 & 0 & 0 & 0 & K_{HSO_4} & -H^+ & 0 & 0 \\ -B(OH)_4^- & 0 & 0 & 0 & 0 & 0 & K_B & -H^+ & 0 & 0 & 0 & 0 \\ -HS^- & 0 & 0 & 0 & 0 & 0 & 0 & 0 & 0 & 0 & K_{H_2S,1} & -H^+ \\ 0 & 0 & 0 & 1 & 1 & 1 & 0 & 0 & 0 & 0 & 0 & 0 \\ 0 & 0 & 0 & 0 & 0 & 0 & 1 & 1 & 0 & 0 & 0 & 0 \\ 0 & 0 & 0 & 0 & 0 & 0 & 0 & 0 & 1 & 1 & 0 & 0 \\ 0 & 0 & 0 & 0 & 0 & 0 & 0 & 0 & 0 & 0 & 1 & 1 \\ -1 & 1 & 0 & 0 & 1 & 2 & 0 & 1 & 1 & 2 & 0 & 1 \end{pmatrix}$$

Table SI-2. Model parameters that remain constant across different runs presented in this paper.

Parameter	Value	Description
$F_{\rm in}$	0.15e-3 Gt C/yr	volcanic CO_2 flux
$\delta_{\rm in}$	-6 permil	volcanic δ^{13}C
ε	-28 permil	organic matter fractionation
$F_{\rm prod,0}$	3.6e-3 Gt C/yr	background production rate
$\alpha_{\rm remin}$	0.99	background remineralization fraction
Alk_0	2300μmol/lit	scale in $CaCO_3$ dissolution
$\tau_{\rm CaCO_3}$	5e3 yr	time scale in $CaCO_3$ dissolution
$\tau_{\rm mixing}$	3e3 yr	ocean mixing time scale
$\tau_{\rm pyrite}$	3e3 yr	pyrite formation time scale
$\tau_{\rm siderite}$	3e3 yr	siderite formation time scale
$V_{\rm ocean}$	1.37e21 liter	ocean volume
Γ	6°C	weathering parameter
$\tau_{\rm ep}$	0.3e6 yr	time scale for imposed perturbation

Table SI-3. Model experiments, specifying parameters which vary among model scenarios presented in the paper and supplementary information. All values correspond to nondimensional amplitudes as follows (equations [SI-7]): U is the nondimensional amplitude of the export production perturbation; α of the increase in sulfate reduction; β of the drop in aerobic remineralization; γ of the drop in oxygenic production; η of the increase in iron remineralization.

	description	Fig	U	α	β	γ	η
run 1	aerobic remineralization	SI-1	13	0	0	1	0
run 2	sulfate and iron	SI-2	25	0.8	0.8	0.2	0.138
run 3	sulfate only	SI-3	73	1	1	0.12	0
run 4	iron only	SI-4	4.7	0	0	0.77	1
run 5	$\delta^{13}C$ w/o CO_2 signal	SI-5	25	0.45	0.8	0.55	0.138
run 6	CO_2 w/o $\delta^{13}C$ signal	SI-6	4.8	0.6	0.8	0.12	0.1
run 7	like 02 with step forcing	SI-7	25	0.8	0.8	0.2	0.138
run 8	like 03 with step forcing	SI-8	73	1	1	0.12	0
run 9	like 04 with step forcing	SI-9	4.7	0	0	0.77	1
run 10	$\Gamma = 5^\circ / \log(2)$	SI-10	25	0.8	0.8	0.2	0.138
run 11	$\Gamma = 3^\circ / \log(2)$	SI-11	25	0.8	0.8	0.2	0.138
run 12	sensitivity to α	SI-12	25	0.7	0.8	0.2	0.138
run 13	sensitivity to α	SI-13	25	0.9	0.8	0.2	0.138
run 14	sensitivity to β	SI-14	25	0.8	0.9	0.2	0.138
run 15	sensitivity to β	SI-15	25	0.8	0.7	0.2	0.138
run 16	sensitivity to γ	SI-16	25	0.8	0.8	0.18	0.138
run 17	sensitivity to γ	SI-17	25	0.8	0.8	0.22	0.138

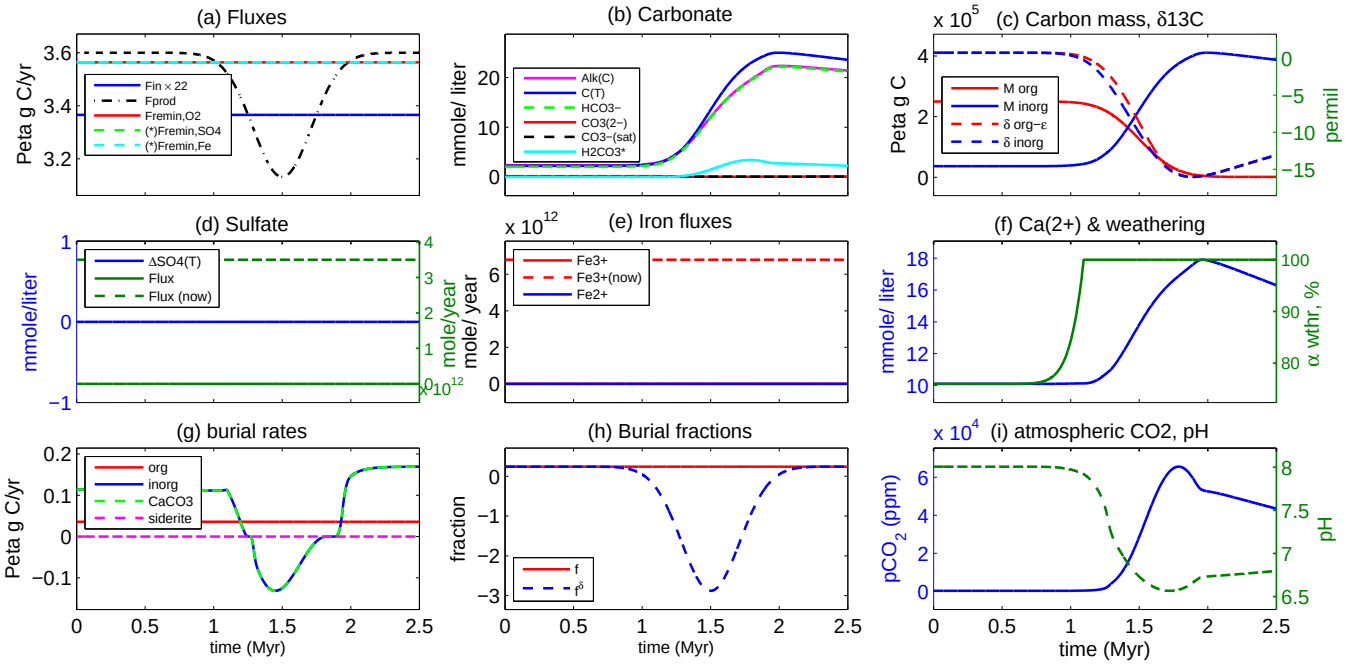

Fig. SI-1. Fuller details of scenario #1 shown in Fig. 1 in the paper, with no iron or sulfate reduction, leading to an isotopic excursion of 15 permil, as well as to a dramatic in crease in pCO_2. The green curve in panel (f) shows the *fraction* of volcanic CO_2 entering the ocean via weathering. The fraction is physically limited to the range (0,1), and in this case reached saturation as calculated following [2]. Please see caption of Fig. 3 in the paper for details.

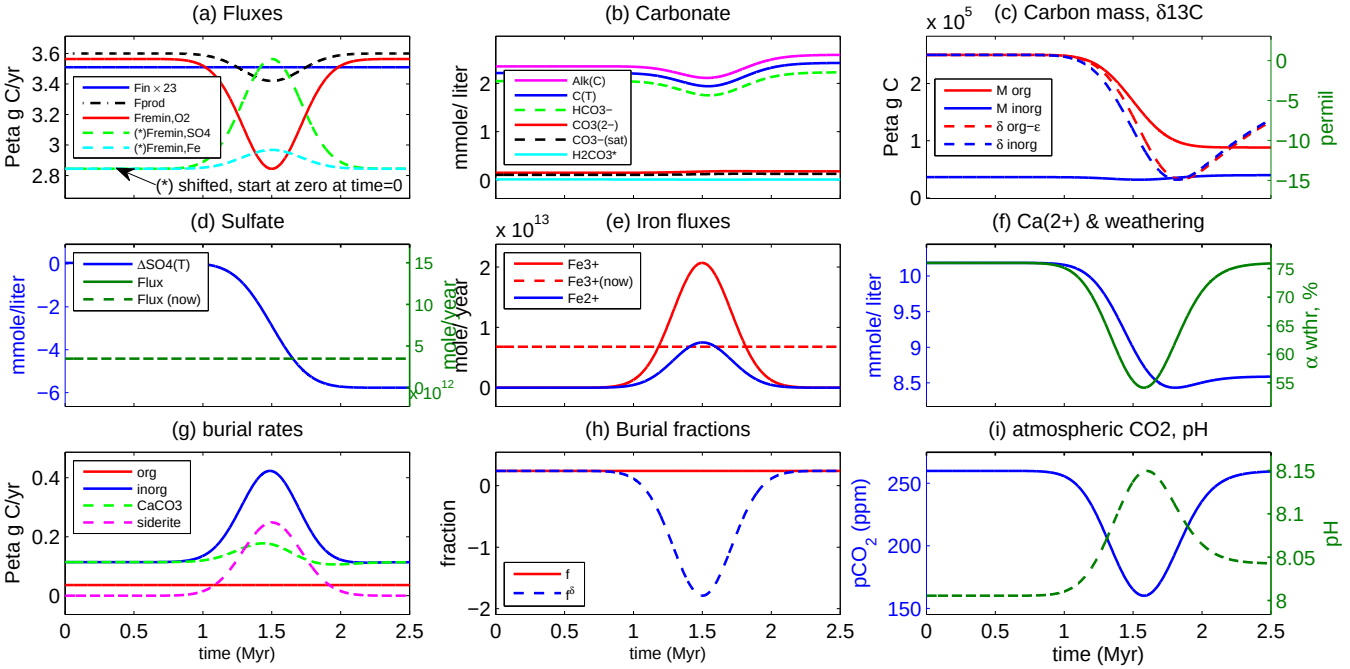

Fig. SI-2. Scenario #2 also shown in Fig. 3 in the paper, with both iron and sulfate reduction, leading to an isotopic excursion of 15 permil, as well as to a decrease in pCO_2.

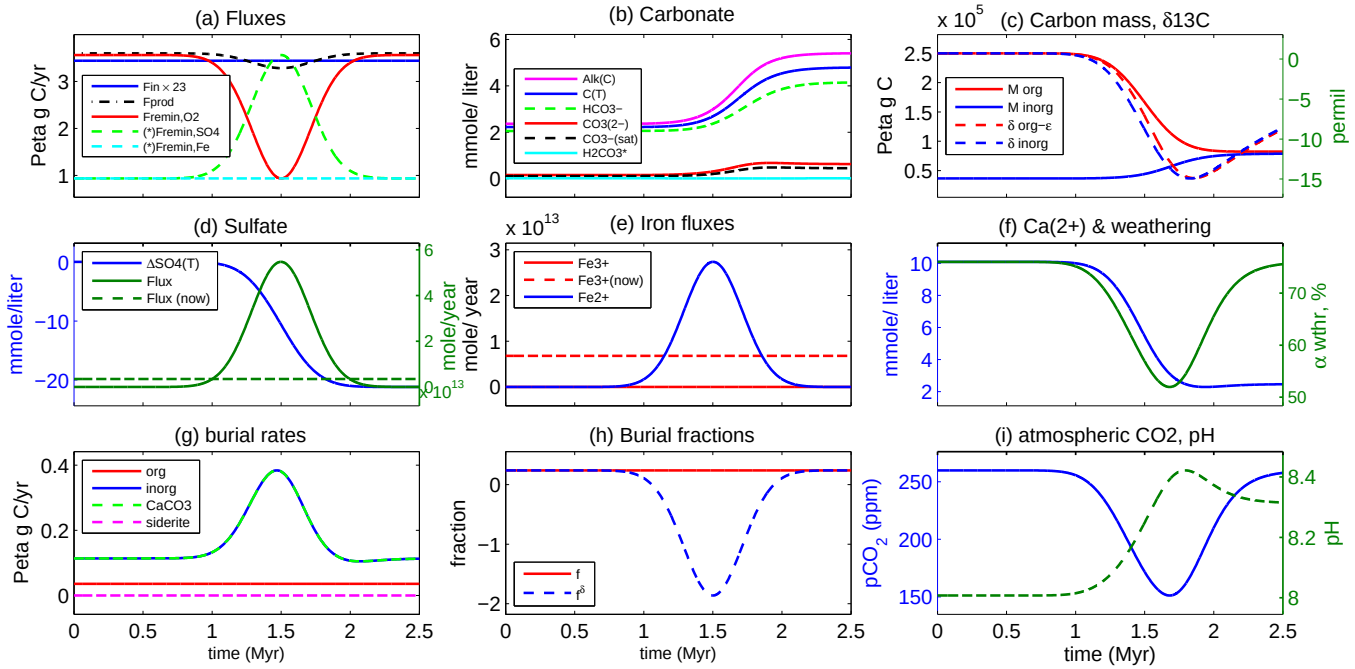

Fig. SI-3. Scenario #3, leading to the same isotopic signal and CO_2 drawdown as scenario #2 of Fig. 3 in the paper, but using only sulfate reduction, and no iron reduction.

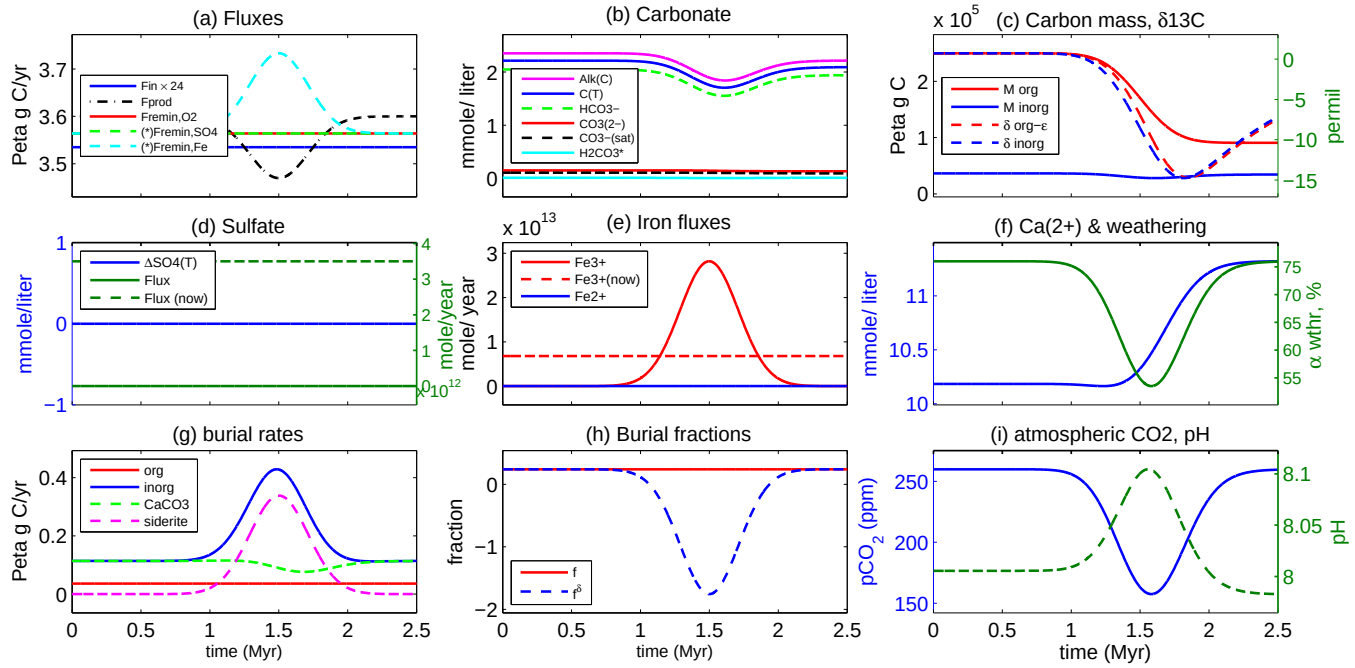

Fig. SI-4. Scenario #4, leading to the same isotopic signal and CO_2 drawdown as scenario #2 of Fig. 3 in the paper, but using only iron reduction, and no sulfate reduction.

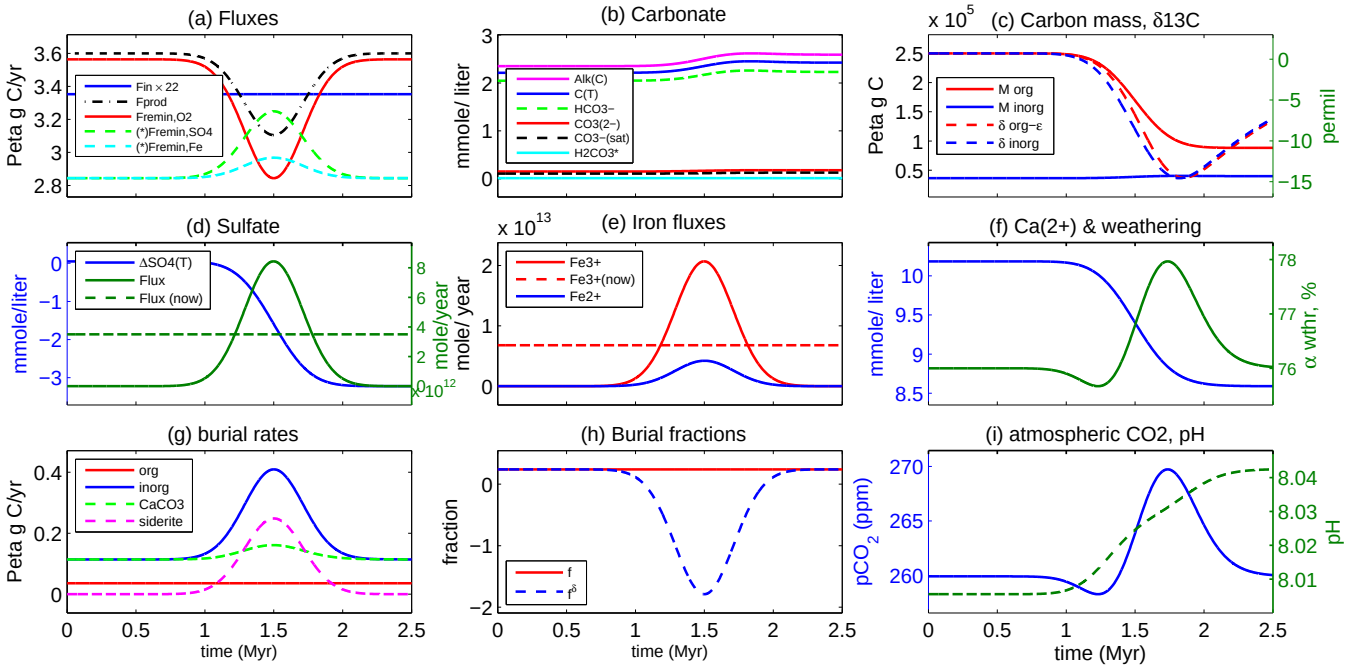

Fig. SI-5. Scenario #5, leading to the same isotopic signal as scenario #2 of Fig. 3 in the paper, but with basically no change to the atmospheric pCO_2.

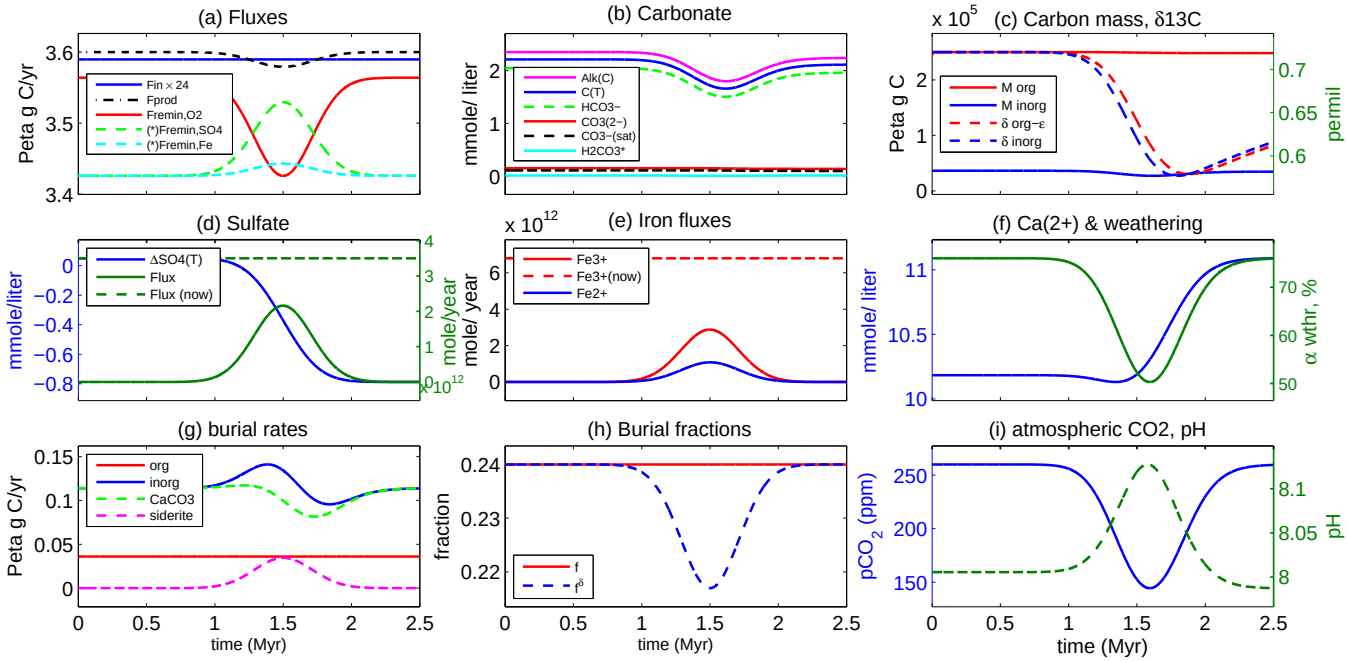

Fig. SI-6. Scenario #6, leading to the same pCO_2 drawdown as scenario #2 of Fig. 3 in the paper, but with practically no isotopic signal.

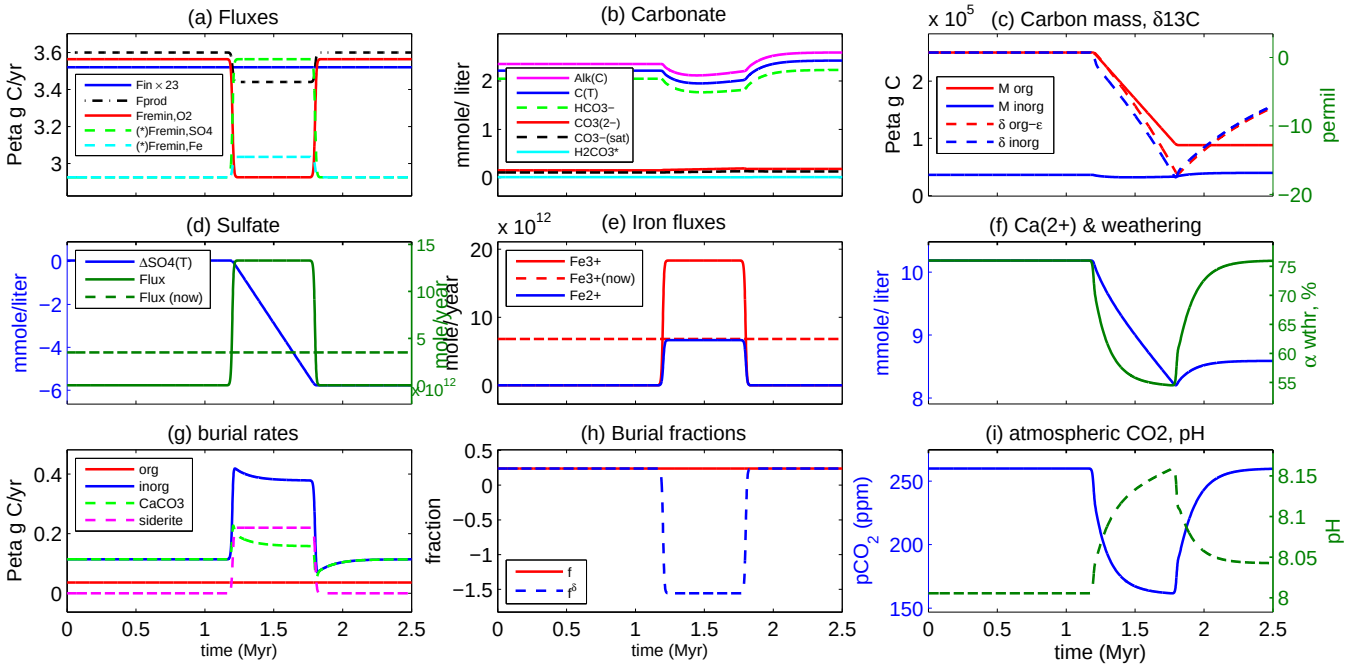

Fig. SI-7. Scenario #7, same as 2, but with step function forcing.

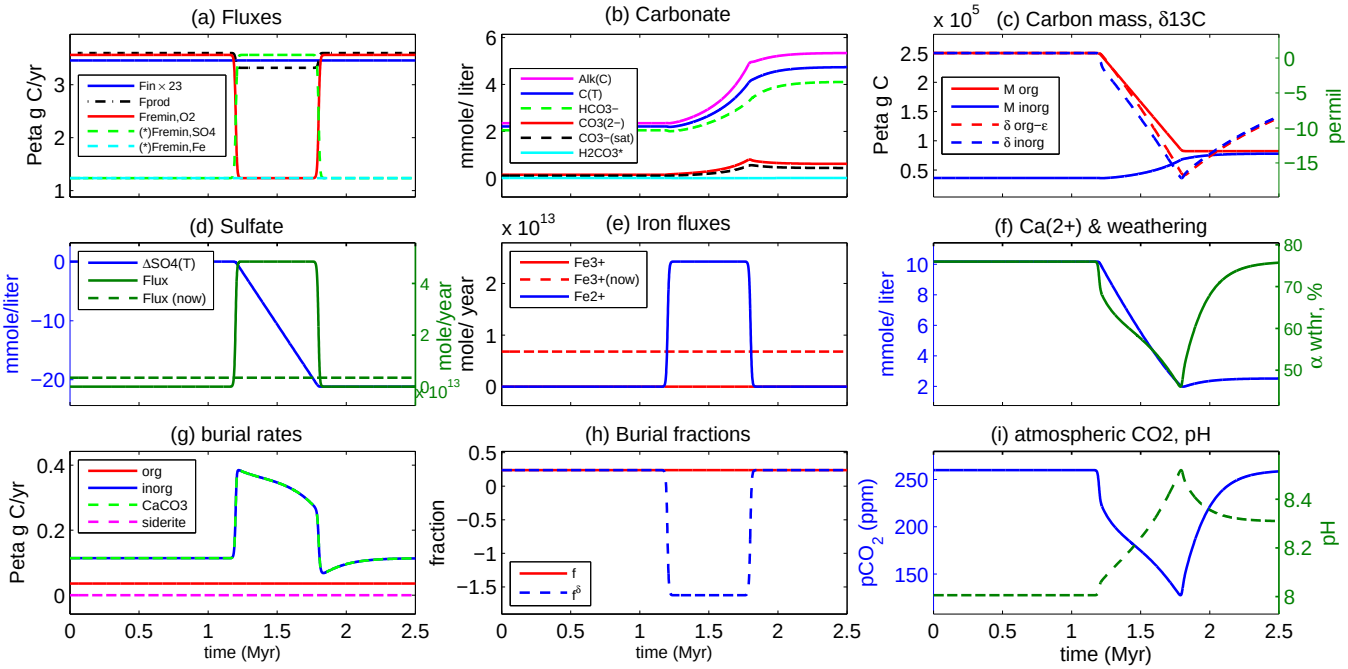

Fig. SI-8. Scenario #8, same as 3, but with step function forcing.

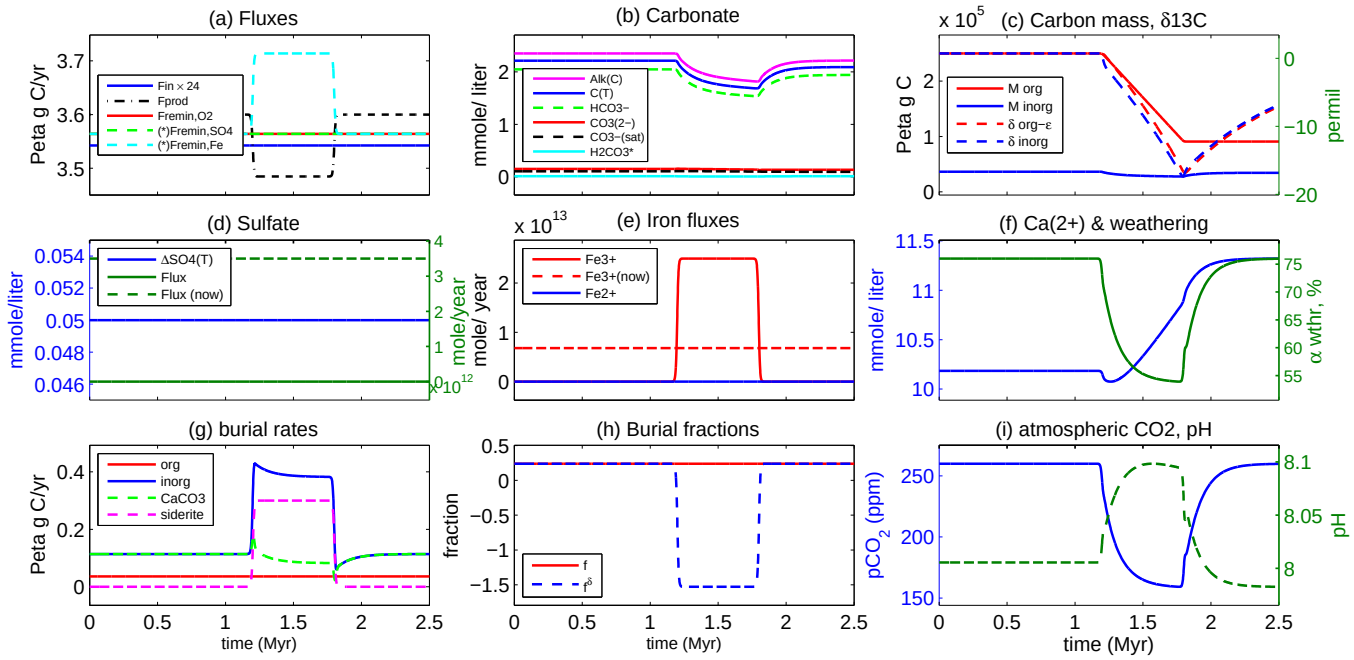

Fig. SI-9. Scenario #9, same as 4, but with step function forcing.

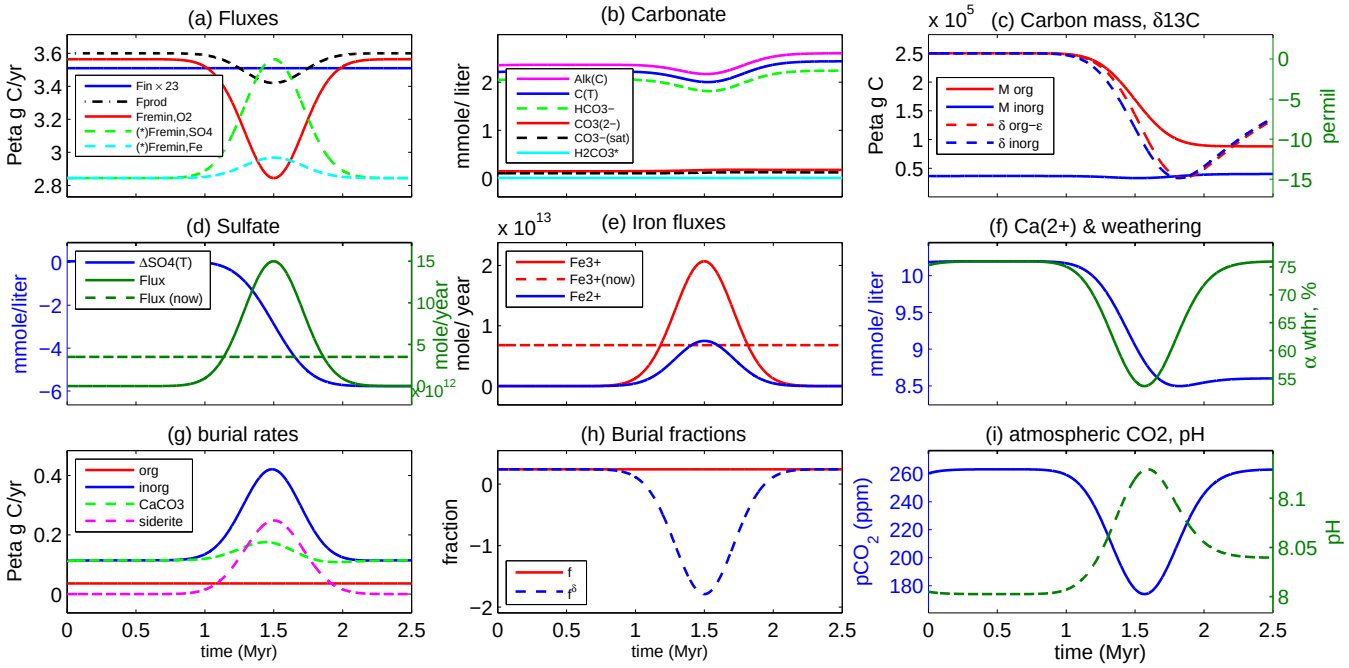

Fig. SI-10. Scenario #10, as in 2, except that climate sensitivity is set to 5 degree C per doubling of CO_2 instead of 4.

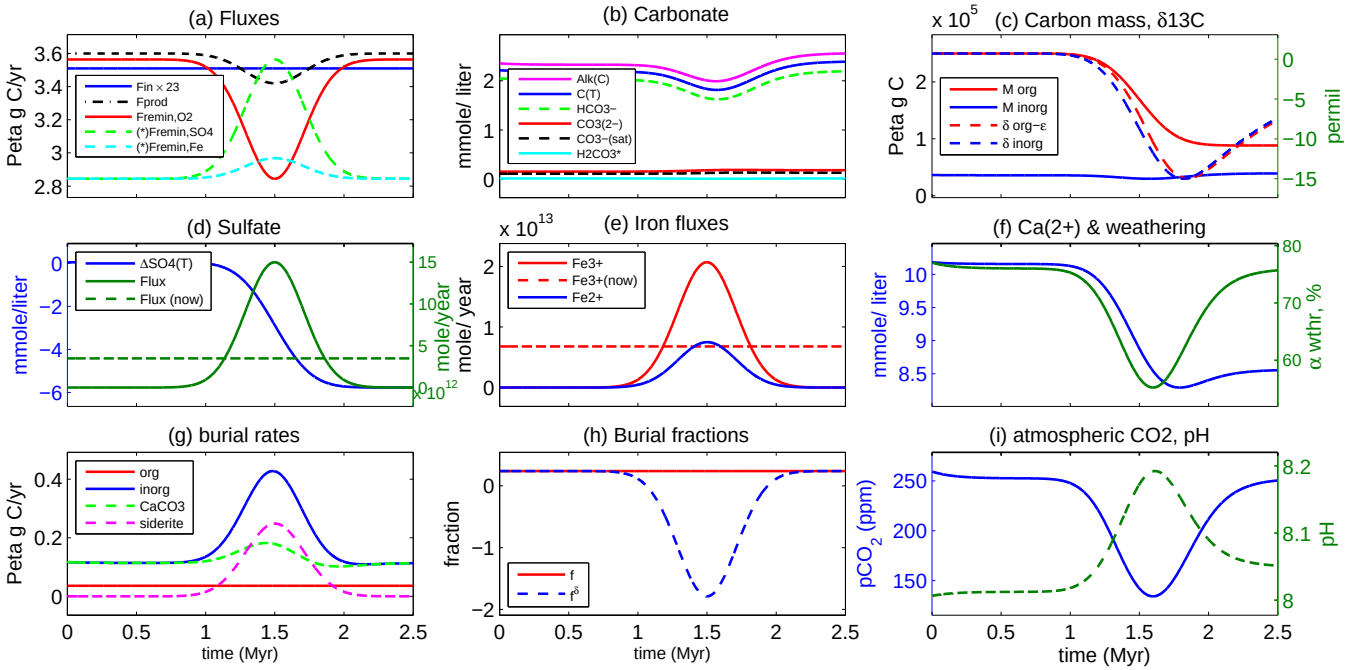

Fig. SI-11. Scenario #11, as in 2, except that climate sensitivity is set to 3 degree C per doubling of CO_2 instead of 4.

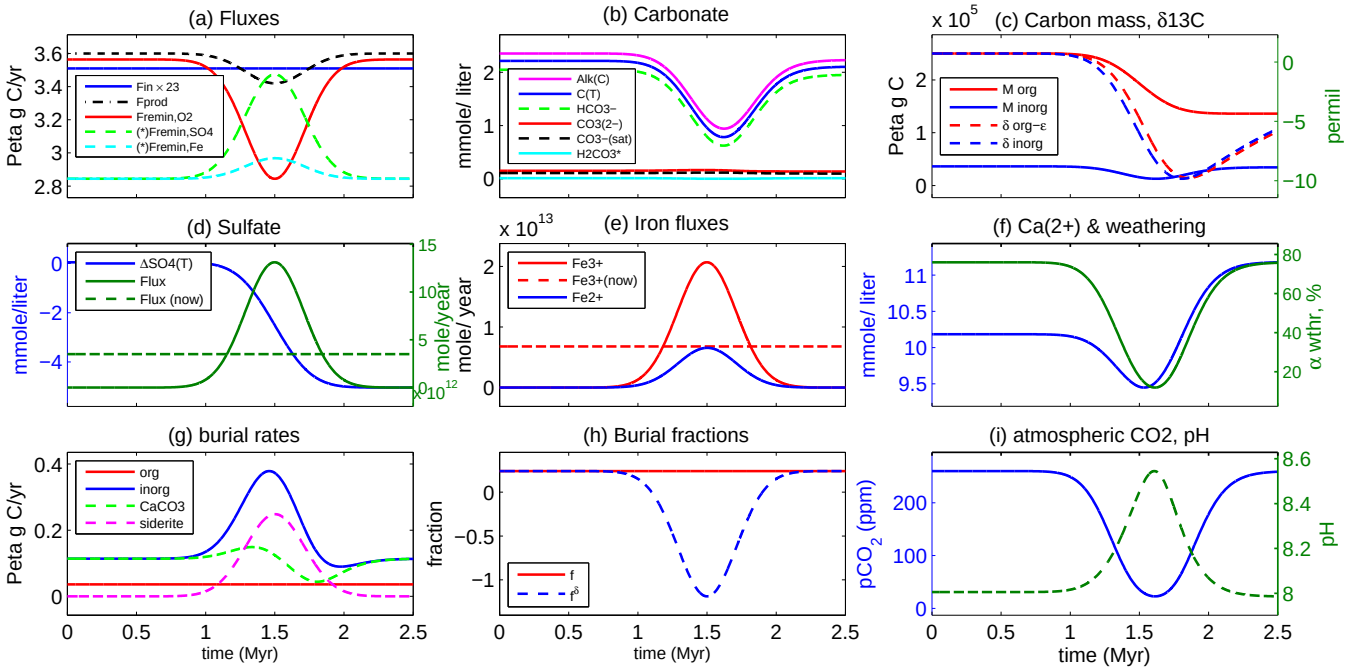

Fig. SI-12. Scenario #12, as in 2, except that sulfate remineralization rate factor is set to $\alpha = 0.7$ instead of 0.8.

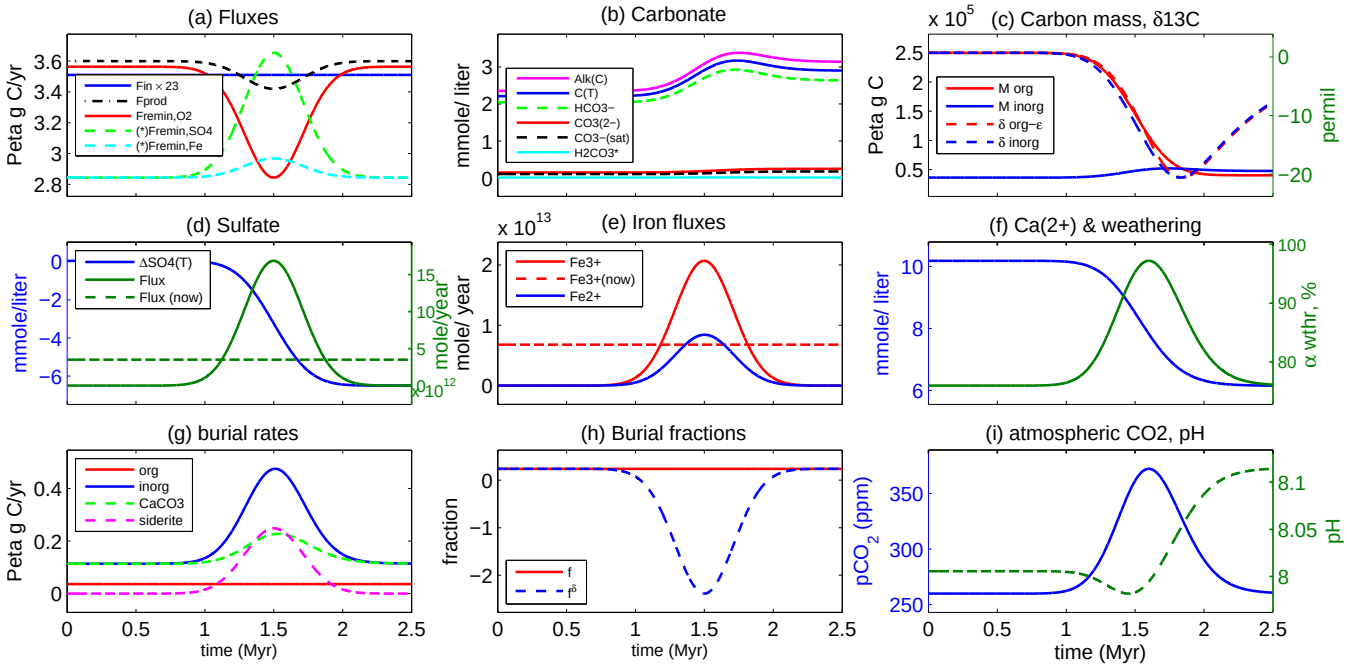

Fig. SI-13. Scenario #13, as in 2, except that sulfate remineralization rate factor is set to $\alpha = 0.9$ instead of 0.8.

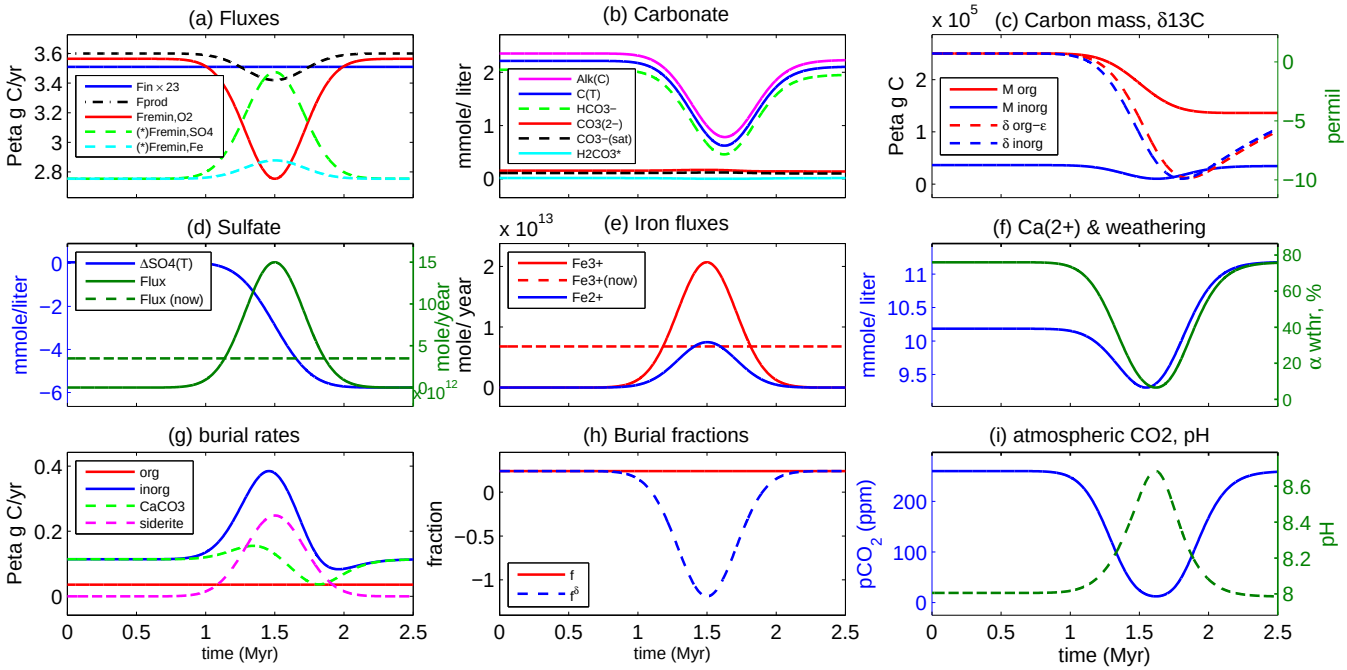

Fig. SI-14. Scenario #14, as in 2, except that the aerobic remineralization rate factor is set to $\beta = 0.9$ instead of 0.8.

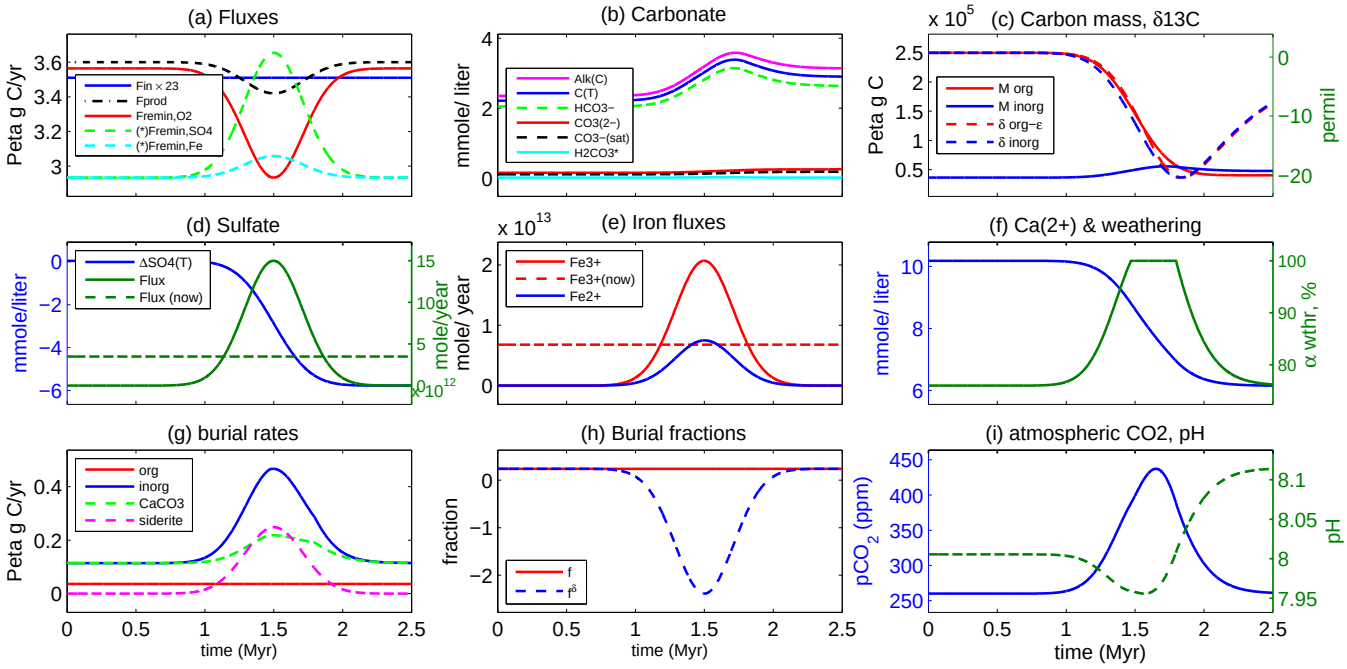

Fig. SI-15. Scenario #15, as in 2, except that the aerobic remineralization rate factor is set to $\beta = 0.7$ instead of 0.8.

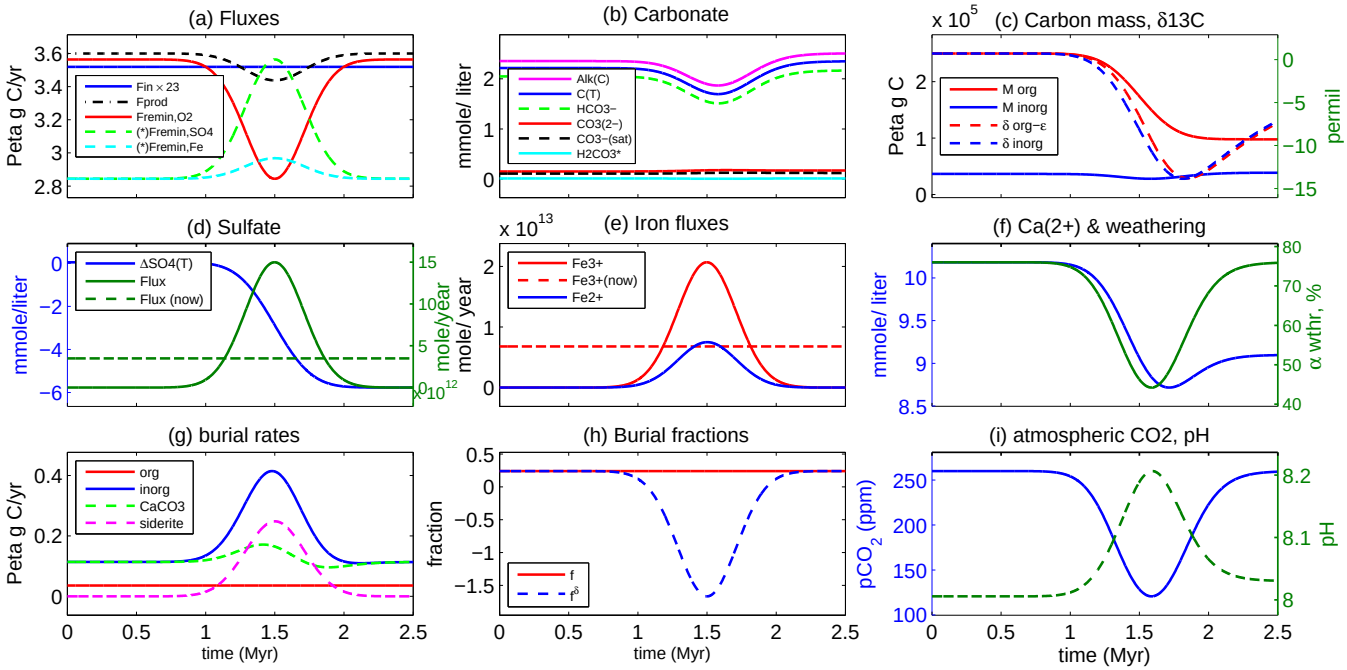

Fig. SI-16. Scenario #16, as in 2, except that the oxygenic production rate factor is set to $\gamma = 0.18$ instead of 0.2.

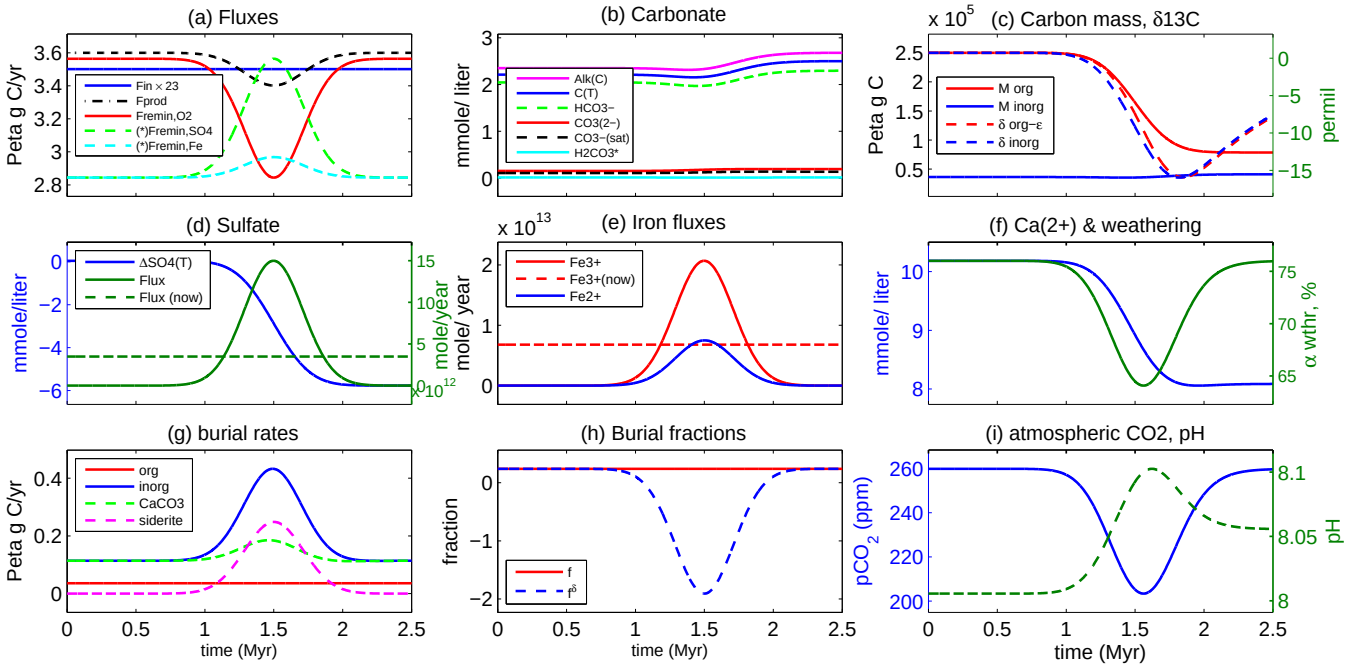

Fig. SI-17. Scenario #17, as in 2, except that the oxygenic production rate factor is set to $\gamma = 0.22$ instead of 0.2.

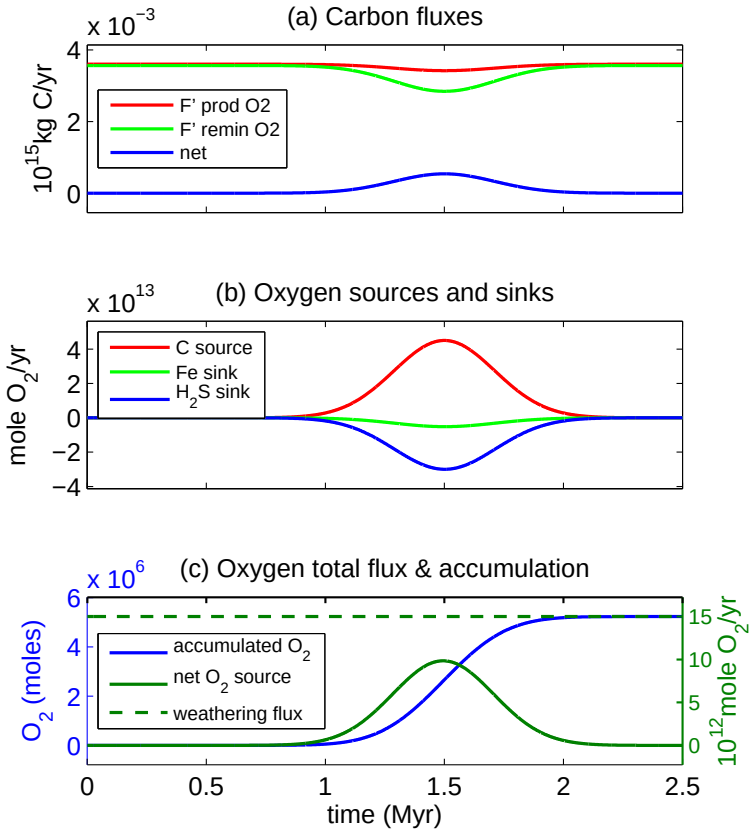

Fig. SI-18. Oxygen consequences of scenario #2. (a) Oxygenic production and remineralization carbon fluxes, and implied net anomalous carbon flux (anomaly in production minus anomaly in remineralization, (section SI-5). (b) Sources and sinks of oxygen due to net oxygenic organic carbon production (red), Fe2+ oxidation (green) and sulfide oxidation (blue). (c) Total O2 source (solid green), present-day weathering sink of O_2 (dashed grin), and the total accumulating O_2 due to the net carbon flux, in the absence of any sinks (solid blue).